HUNGARIAN GROUP OF *fib*

CONCRETE STRUCTURES

ANNUAL TECHNICAL JOURNAL

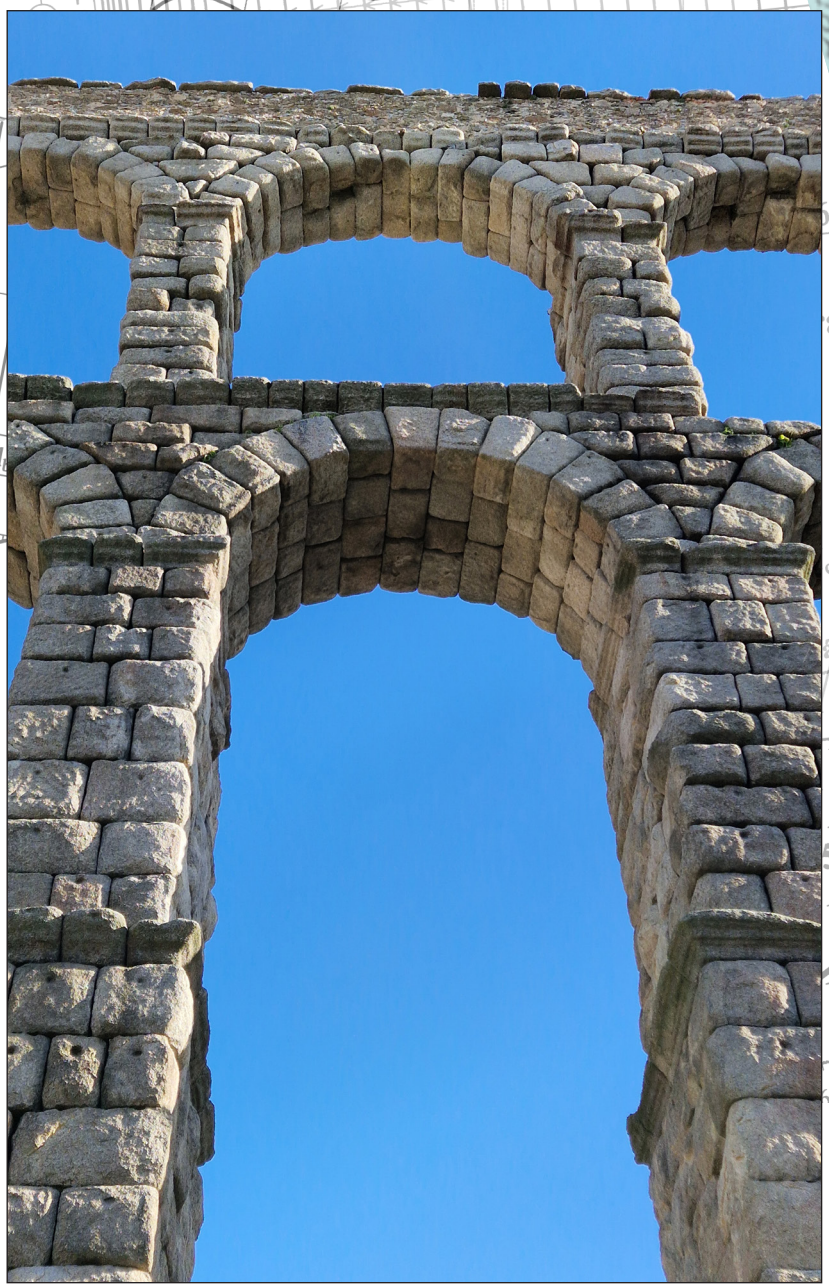

2024

Vol. 25

Since 1942

LÁBATLANI VASBETONIPARI ZRT.

Member of the RAILONE GROUP



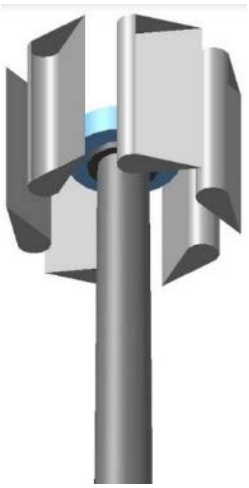



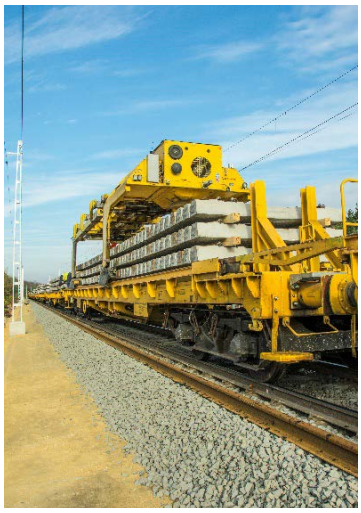


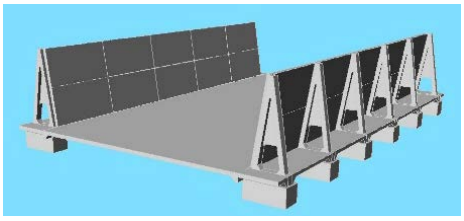

#railway sleepers #turnout sleepers #narrow gauge sleepers #platform elements #panel elements for urban transit #composite sleepers #lighting poles #upperline poles #wind generator poles #energy poles #agricultural elements #fence elements #statue pedestal and other unique products

Lábatlani Vasbetonipari Zrt. www.railone.hu

CONCRETE STRUCTURES
Journal of the Hungarian Group of ***fib***

Founded by: Hungarian Group of ***fib***
Publisher: Hungarian Group of ***fib***
(***fib*** = International Federation for Structural Concrete)

Editorial office:
Budapest University of Technology and Economics (BME)
Department of Construction Materials and Technoligies
Műegyetem rkp. 3., H-1111 Budapest
Phone: +36-1-463 4068
Fax: +36-1-463 3450
WEB http://www.fib.bme.hu
WEB editor: András Bíró

Layout and print: Csaba Halmai, Navigar Ltd.

Printed in 100 copies and web.

HU ISSN 2062-7904
online ISSN: 1586-0361

Cover photo:
Roman aqueduct in Segovia, Spain.
Photo: György L. Balázs

CONTENT

ROLE OF CONNCECTED MEMBERS ON THE LOAD BEARING CAPACITY OF COMPRESSED RC COLUMNS - VALIDATION OF CONSTEEL'S METHOD



https://doi.org/10.32970/CS.2024.1.1

Szabolcs Szinvai - Bálint Vaszilievits-Sömjén - Tamás Kovács

Reinforced concrete (RC) columns are crucial in construction, yet their design is challenging. Design typically involves first-order analysis, consideration of imperfections, and calculation of second-order effects, often done on an isolated column for simplicity, without precise consideration of adjacent elements. Although this approach is generally effective, it can lead to serious errors in certain cases. To investigate this problem, single columns under axial compression with different support conditions were first evaluated, followed by two columns connected by a stiff beam with hinged connections. The columns studied were either loaded at different intensities, had different boundary conditions, or had different cross-sectional areas. The evaluations included the nominal curvature method; the automatic nominal curvature method in ConSteel, which is a novel approximation of the second-order bending moments based on buckling shapes; and the general method. The results showed that if there is a significant difference in stiffness or in loading intensity between the connected members, the nominal curvature method can underestimate the bending moments compared to the general method. Therefore, in the case of irregular structures, more precise consideration of adjacent elements during design is essential to ensure safety. It was shown that this can be done automatically using the automatic nominal curvature method in ConSteel.

Keywords: second-order effects, nonlinear analysis, column, interaction

1. INTRODUCTION

In contemporary architectural design, slender columns are increasingly favoured due to their efficiency in material use and their ability to enhance spatial utility within interiors. These slender, compressed structural members are susceptible to pronounced second-order effects and require careful evaluation.

The Eurocode 2 standard (EN 1992-1-1, 2004) allows the application of three methodologies for the computation of second-order effects. The nominal curvature (NC) and nominal stiffness (NS) methods are prevalently employed by designers. These approaches are characterised by their simplified and deterministic nature.

The third approach is the general nonlinear method (GM), which is regarded as a more precise design strategy and considered one of the most accurate methodologies available. However, this method is rendered impractical due to its inherent complexity and the challenges it poses in practical application.

The nominal curvature and nominal stiffness approaches give significantly different results. The applicability of the nominal stiffness approach is limited to scenarios where the design load is considerably lower than the buckling load or where the column exhibits minimal slenderness (Araújo, 2017). However, the nominal curvature approach also provides effective results for slender columns. This method uses the slenderness ratio. In cases where the column has marginal slenderness in a particular direction, second-order effects may be disregarded in that direction. This makes it easier to deal with different types of columns.

Many software applications have incorporated these two simplified solutions. Certain applications have implemented these methods with a high degree of precision, adhering strictly to the Eurocode standards. In contrast, other applications have attempted to exploit computational capabilities either by extending the simplified methods or by using a variant of the GM method.

As the construction of increasingly large and more complex structures becomes more prevalent, so does the reliance on automated software solutions. These solutions must be able to address imperfections and second-order effects. A significant advantage of the NS method in this context is its ability to analyse a column as an integral part of the overall structure, rather than treating it as a separated element. This ability can have a significant impact in scenarios where there are significant irregularities in the structure or loading conditions.

In an attempt to retain the advantages of the NC method while extending its applicability to the assessment of column interactions with surrounding structural components, ConSteel has developed an approach that uses the global buckling configuration of the structure to determine the distribution of second-order bending moments more accurately. This paper attempts to compare three methods: the Eurocode 2 nominal curvature method (manual calculation), the ConSteel automatic nominal curvature method (aNC) and

the GM method implemented within the ATENA software.

The nominal curvature method has faced criticism from researchers since its introduction in Eurocode 2 (EN 1992-1-1, 2004). Critics often highlight that the method yields conservative outcomes due to an overestimation of curvature in certain scenarios. Therefore, attempts were made to improve the precision of this method.

Barros (Barros et al., 2010) proposed an improved nominal curvature method, where the curvature is interpolated between the steel yield conditions and the maximum allowable curvature, depending on the axial load. For concrete classes above C60, the scenario in which both steel yields prevail is unattainable, resulting in a curvature being lower than the values prescribed in Eurocode 2.

Kollár, Csuka, and Ther (Kollár et al., 2014) remarked that concentrically loaded columns are not addressed in a distinct way. Eurocode introduces a "capacity reduction factor" for materials such as masonry, timber, and steel to facilitate calculations for concentrically loaded columns. Consequently, they have proposed formulae for determining the load-bearing capacity of such columns, claiming that their methodology is simpler and more precise than the simplified methods in Eurocode.

With the constant improvement of computational capacity, the general method can be seen as a valid alternative to improve accuracy. However, even if it is considered to be more accurate, its reliability is questionable. A primary concern is that stability failure can occur at reduced concrete stress and deformation (Fig. 1, right). In this context, due to the nonlinear stress-strain diagram inherent in the GM method, there is a reduced margin of safety compared to that when failure is due to concrete crushing. For stability failure, the dominant partial safety factor exerting influence is γ_{CE}, which reduces the Young's modulus of concrete. Alternatively, to more accurately address this issue, probabilistic analysis methods can be used, including the estimation method of coefficient of variation (ECOV), which have been proposed by researchers such as Wolinski (Wolinski, 2011) and Cervenka (Cervenka, 2013).

Dobry (Dobry et al., 2022) conducted laboratory experiments and developed numerical models to explore the probability of unsafe design consequences due to the use of the GM method. His findings indicated that employing the GM method absent laboratory test calibration culminates in a 47% disparity between the maximum and minimum buckling force. This is attributable to uncertainties related to material properties, dimensions, and nonlinear compressive structural behaviour. This uncertainty raises questions regarding the feasibility of using the GM method safely in design applications, necessitating the incorporation of additional safety measures in design contexts where GM methods are applied.

This confirms the premise that simplified methods are appropriate for practical routine design applications.

2. PROBLEM STATEMENT

The nominal curvature method does not precisely take into account the interaction of adjacent columns, which places the responsibility on the designer to correct the calculations when necessary. ConSteel's novel method, called the automatic nominal curvature method, claims to be able to handle this issue automatically, which can prevent designer errors. Detailed information on this method can be found in ConSteel's knowledge base article (ConSteel, 2023).

The main objective of this paper is to validate the ConSteel method and to further emphasise the possible errors that can occur during the design of irregular structural systems. Three distinct computational approaches were compared: (1) an analytical calculation in accordance with Eurocode 2, using the nominal curvature method; (2) finite element modelling within ConSteel, applying a novel approximation of second-order bending moments based on buckling shapes, described in the software as the 'automatic nominal curvature' method; (3) the general method using geometrically nonlinear analysis performed in the ATENA software. The three methods handle geometric nonlinearity and imperfections with different levels of precision. Further aim of this study is to show the effects of more precise considerations on the load bearing capacity of reinforced concrete columns.

Fig. 1: *Stability failure of slender columns (left), concrete stress-strain diagram with mean and design values (right) (Dobry et al., 2022)*

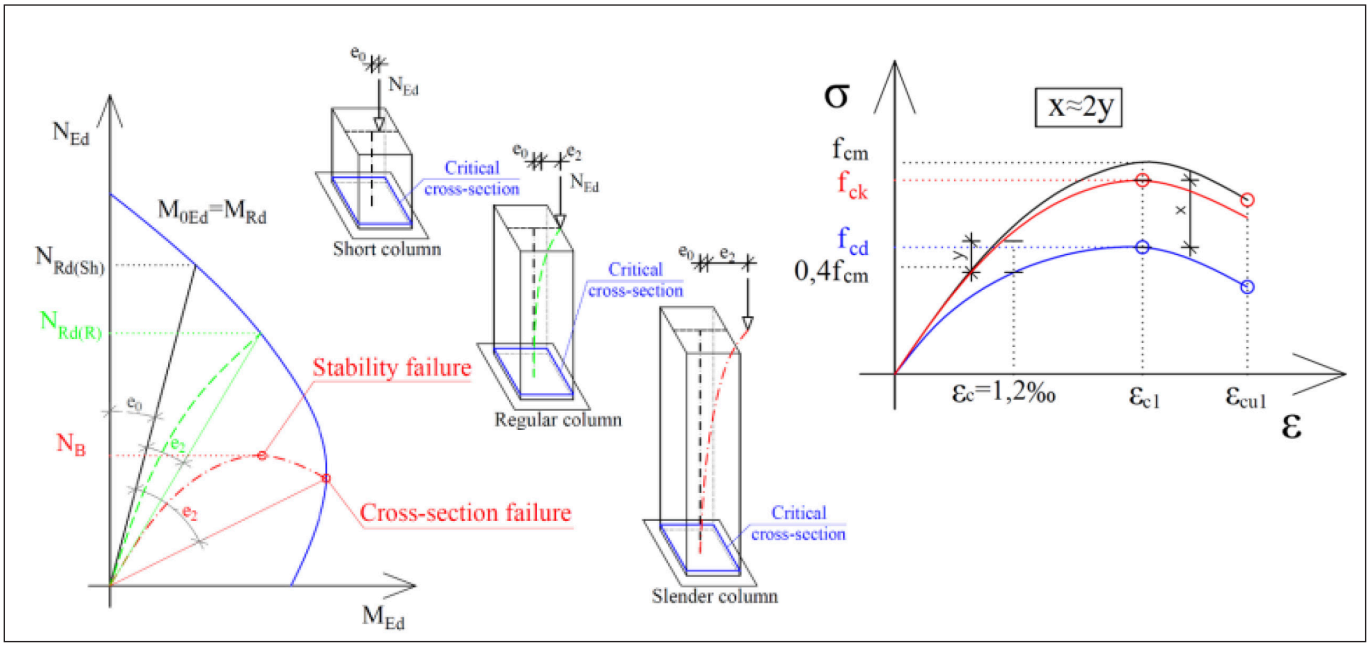

3. APPROACH

To investigate the problem, single columns under axial compression with different support conditions were first evaluated, followed by two columns connected by a stiff beam with hinged connections. The columns studied were either loaded at different intensities, had different boundary conditions, or had different cross-sectional areas.

An imperfection of 1/200 of the height of the columns was taken into account in all three calculations. In the case of the NC and aNC methods, this imperfection was taken into account with a horizontal load, whereas in the GM method the geometry was defined in an imperfect way. The distribution of the imperfection followed the buckling shape of the column (which was dependent on the boundary conditions) where the maximum intensity was equal to 1/200 of the height of the columns.

The effect of curvature was taken into account in the NC case by the second-order bending moment, with a uniform distribution, while in the aNC case, the distribution of the second-order bending moment was determined based on linear buckling analysis (LBA).). The GM method automatically considered the curvatures by geometrically nonlinear analysis.

In the NC case, a first-order analysis was sufficient, while in the aNC case a LBA and also a buckling sensitivity analysis was necessary. LBA is needed to calculate the distribution of the curvatures, and buckling sensitivity analysis is essential, since the software uses the results of this analysis to assign the correct buckling shapes for each column. In the aNC method, interaction between structural elements is taken into account by the LBA, whereas the GM method uses geometrically nonlinear analysis.

Creep in the NC and aNC methods is considered using the final value of the creep coefficient , to calculate factor , which is then used to calculate the curvature. In the GM method creep is considered in a simplified way, by using the effective design value of the Young's modulus of concrete (), where the final value of the creep coefficient is the same as previously used for the NC and aNC methods.

The maximum load bearing capacity of the columns for each problem was determined using the N-M biaxial bending interaction diagram for the NC and aNC methods, and by the maximum point of the load-displacement curve for the GM.

4. NUMERICAL MODELS

Initially, single column scenarios were tested. The simplicity of these cases allowed for the comparison of the three computational methods and the calibration of the parameters used. The objective was to obtain comparable results at failure under conditions of maximum loading and maximum curvature. The notation for each case and the boundary conditions are summarised in Table 1.

Having achieved similar results in three types of evaluation using single-column models, identical models were then used to construct two column frames. The apices of the columns were connected by a rigid beam, incorporating hinged connections, as shown in Fig. 2 (middle). The sole function of this element is to facilitate the transfer of loads between the two columns.

A comprehensive analysis was carried out that included five different cases. First, identical columns with fixed-free boundary conditions were subjected to equivalent loading intensities at the top. This approach was intended for validation purposes, and the expected result reflected the results obtained when testing single columns under similar boundary conditions. In the second scenario, the loading conditions were changed so that only one column was subjected to a load, while the adjoining column remained unloaded, but was subjected to lateral forces from the connected column. In the third scenario, both columns were loaded; however, one column was subjected to only half the load intensity. In the fourth scenario, the conditions were the same as in the first scenario, but the columns were designed with cross-sectional areas that provided a bending stiffness ratio of one to five between them. The final and fifth scenarios maintained the conditions of the first but introduced a variation in the support conditions: One column had a hinged bottom support, while the other column retained a fixed support. The notations for the two-column scenarios are summarised in Table 2.

4.1 Geometry

The columns considered in our calculations were each 6.00 metres high and had a cross-sectional area of 400 by 400 millimetres. The reinforcement specifications included a concrete cover of 3 centimetres, four longitudinal steel bars with a diameter of 28 millimetres and stirrups with a diameter of 10 millimetres, uniformly distributed at 200 millimetre intervals.

The geometry of the models is shown in Fig. 2. In models with different bending stiffness between the two columns, a ratio of 1:5 was achieved by reducing the dimensions of

Table 1: *Summary of single column calculation cases*

Single columns			
Method	Notation	Bottom support	Top support
Eurocode 2: Nominal Curvature Method	NC_cant	fix	free
	NC_ss	hinged	hinged
	NC_bs	fix	hinged
ConSteel: Automatic Nominal Curvature Method	aNC_cant	fix	free
	aNC_ss	hinged	hinged
	aNC_bs	fix	hinged
Eurocode 2: General Method – ATENA	GM_cant	fix	free
	GM_ss	hinged	hinged
	GM_bs	fix	hinged

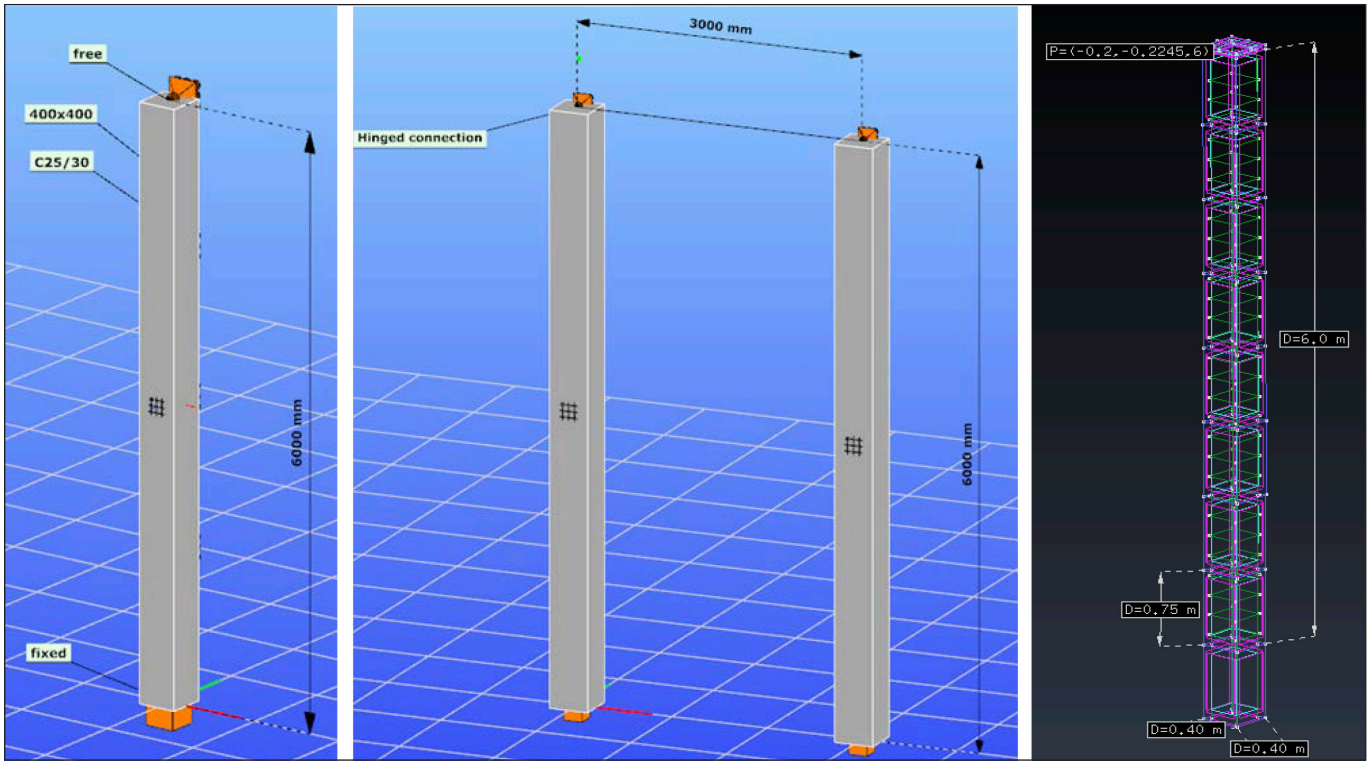

Fig. 2: Geometry of models: single cantilever in ConSteel (left), two-column frame in ConSteel (middle), and single cantilever in ATENA (right).

Table 2: Summary of two-column frame calculation cases

Two-column frames		
Method	Notation	Description
Eurocode 2: Nominal Curvature Method	NC_PP	Identical columns, identical loading. For model validation.
	NC_P0	Identical columns, only one is loaded.
	NC_2PP	Identical columns, one column is loaded twice as much as the other one.
	NC_EI	Bending stiffness ratio between the columns is 1:5, identical loading.
	NC_SS	Identical columns, identical loading, one column is simply supported.
ConSteel: Automatic Nominal Curvature Method	aNC_PP	Identical columns, identical loading. For model validation.
	aNC_P0	Identical columns, only one is loaded.
	aNC_2PP	Identical columns, one column is loaded twice as much as the other one.
	aNC_EI	Bending stiffness ratio between the columns is 1:5, identical loading.
	aNC_SS	Identical columns, identical loading, one column is simply supported.
Eurocode 2: General Method - ATENA	GM_PP	Identical columns, identical loading. For model validation.
	GM_P0	Identical columns, only one is loaded.
	GM_2PP	Identical columns; one column is loaded twice as much as the other one.
	GM_EI	The bending stiffness ratio between the columns is 1:5, identical loading.
	GM_SS	Identical columns, identical loading; one column is simply supported.

one column to 267.5×267.5 mm. Consequently, the inertia ratio of the columns is 1:5, while their modulus of elasticity remains constant. In the NC and aNC scenarios, columns were specified with ideal geometry, and imperfections were accounted for by horizontal loads (see Chapter 3.3). In the GM approach, it was necessary to model the structure with its imperfect geometry to conduct an imperfect analysis. The imperfect geometry followed the buckling shape of the column, where the largest displacement value was equal to 1/200 of the height of the column. In ATENA, solid elements were utilised for concrete, while so-called 1D bar elements were used for reinforcement. The centre line of the reinforcement bars was modelled. Additional plates were incorporated as volume elements for loading purposes. Anticipating failure in the cantilever column in the bottom section, the columns were extended to provide a continuous mesh at the base. The 6.00 m column was subdivided into eight sections, each 750 mm in length. Each square-based prism was offset by 1/8 of the imperfection value to form a parallelepiped. This was essential to ensure the accuracy of the model. The use of a curved line would have precluded the use of hexahedral elements for meshing. In instances involving two columns, the rigid beam was modelled as a solid steel beam that employs solid elements. This element had adequate stiffness and facilitated the definition of the necessary loads and connections.

4.2 Materials

In the calculations, C25/30 grade concrete and B500B reinforcement were used. The design for the modulus of elasticity of the concrete was used as specified:

$$E_{cd} = E_{cm}/\gamma_{cE}, \quad (1)$$

where is the mean value of the modulus of elasticity, and is the partial safety factor for the modulus of elasticity of concrete.

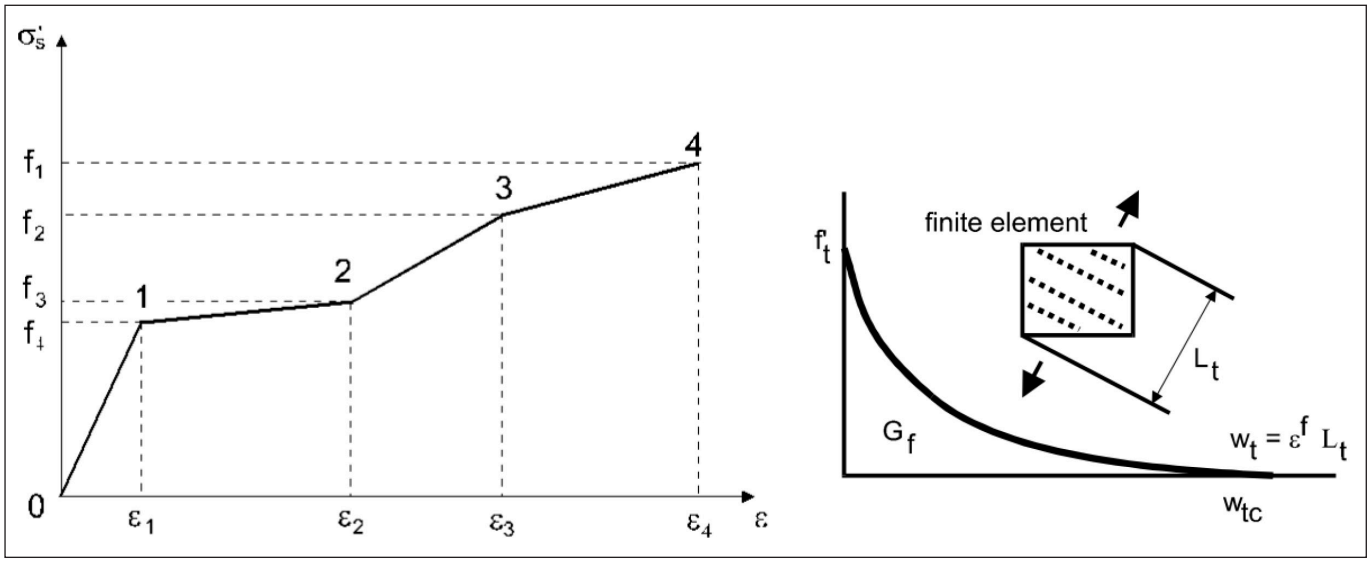

Fig. 3: *Multilinear stress-strain law (left), tensile softening, and characteristic length (right) (Cervenka et al., 2020)*

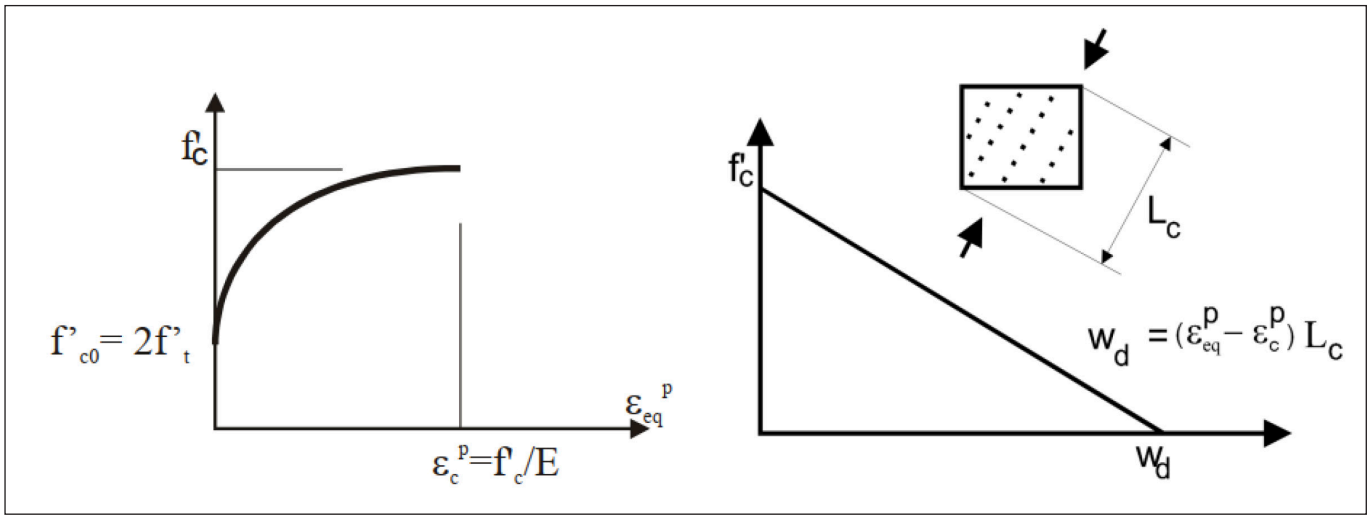

Fig. 4: *Compressive hardening/softening and compressive characteristic length. Based on experimental observations by Van Mier (Cervenka et al., 2020)*

In the NC and aNC scenarios, linear isotropic material models were used. In these cases, the consideration of creep in the calculations of the second-order bending moments negated the need for further modifications. The GM method was used to account for material nonlinearity. The multilinear stress-strain law was applied to the reinforcement as shown in Fig. 3 (left). This multilinear approach consists of four segments and facilitates the modelling of all four stages of steel behaviour: elastic state, yield plateau, hardening, and fracture. For B500B steel, a modulus of elasticity of 200 GPa and a design yield strength of 435 MPa were used.

In the study, the ATENA CC3DNonLinCementitous2 material model was used for the concrete analysis. This model integrates a fracture-plastic framework that combines constitutive approaches for tensile (fracture) and compressive (plastic) behaviours. The fracture mechanism is based on an orthotropic smeared crack formulation paired with a crack band model. It accommodates both the rotated and fixed crack models, and our analysis utilises the fixed crack model. As depicted in Fig. 3 (right), the size of the crack band, denoted L_c, is determined by projecting the size element in the direction of the crack. Fig. 4 illustrates the compressive behaviour, where the ascending (hardening) phase is characterised by an elliptical shape, while the descending (softening) phase follows a linear trajectory. The governing equation for the ascending branch is strain-based, whereas the descending branch is displacement-driven to address issues related to mesh size.

In our models, the interface between the concrete and the reinforcement is rigidly established, indicating the absence of slippage. The nodes associated with the one-dimensional elements are systematically generated to ensure alignment at the boundaries with the concrete elements.

To consider the effect of creep, the effective modulus of elasticity of concrete was used in GM models:

$$E_{\mathrm{cd,eff}} = \frac{E_{\mathrm{cm}}}{\gamma_{\mathrm{cE}}\left(1+\varphi(\infty,t_0)\right)}, \qquad (2)$$

where is the same value as later used in Consteel calculations (for curvature).

4.3. Boundary Conditions

In the examination of planar scenarios, all models are supported in the y direction, while the x-z plane is under investigation. To establish a fixed column end in the GM method, support was defined on the lower surface of the 6.00 metre column in the x, y and z directions. To create a hinge between the solid steel beam and the top loading plate, only the centreline of the loading surface was connected to the

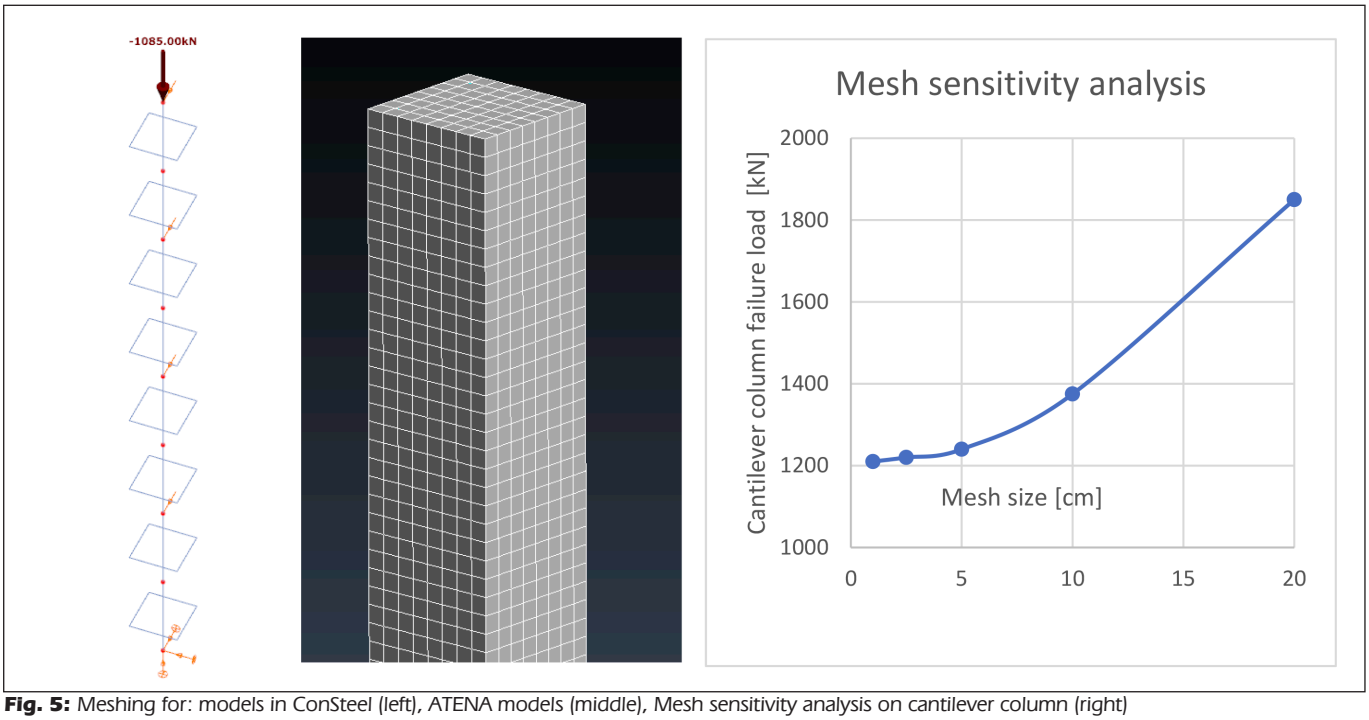

Fig. 5: *Meshing for: models in ConSteel (left), ATENA models (middle), Mesh sensitivity analysis on cantilever column (right)*

steel beam. Vertical loads were applied axially to the top of the columns, ignoring the self-weight. In both the NC and aNC cases, horizontal loads were characterised by a 1/200 imperfection (using the height of the column). The magnitude of the vertical loads increased progressively in all scenarios, until structural failure occurred, as indicated by the crushing of the concrete (see Chapter 3.5). In ConSteel, the support conditions were specified using the point support function.

4.4 Mesh

For the aNC models, the automatic mesh size suggested by ConSteel was utilised, resulting in the formation of elements measuring 75 cm in length with the software employing 8 meshes. The GM models incorporated hexahedral elements with an edge length of 5 cm. This dimension was derived from the mesh sensitivity analysis (Fig. 5 on the right) conducted on the single cantilever column, where mesh sizes ranging from 1 to 20 cm were examined. A 5 cm mesh size was selected because it yielded a discrepancy of less than 1% compared to the converged failure load.

4.5 Analysis parameters

Several analyses had to be performed in order to handle the aNC cases. First-order, buckling, and buckling sensitivity analyses were performed. It was imperative to verify the corresponding buckling modes assigned to the columns. Through the employment of the GM methodology, a Geometrically and Materially Nonlinear Imperfect Analysis (GMNIA) was intended. Imperfections were incorporated in the geometric definition as outlined in Chapter 3.1, while material nonlinearity was addressed as per the explanation in Chapter 3.2. Nonlinear analysis was conducted using the Arc-Length method, which was favoured over the Newton-Raphson method due to its suitability for load-controlled numerical experiments. This method also facilitated the investigation of the descending branch of the phenomenon. The Elastic Predictor was employed to compute between iterations, whereas the Pardiso solver was used for matrix solutions. A load increment of 10 kN was applied. Under these conditions, satisfactory mathematical convergence was achieved, with most iterative steps converging in under ten iterations. However, as the failure load was approached, an increase in the number of iterations was observed.

5. RESULTS

An evaluation was carried out on three main characteristics. Initially, the curvature and the second-order bending moments were examined to acquire a comprehensive understanding of the behaviour. Subsequently, the failure modes of the columns were analysed along with the identification of the specific column that failed. Ultimately, the failure load associated with the various methodologies and cases was systematically compared.

5.1 Curvature

A comprehensive visualisation of the curvatures is presented in the Appendix. A single figure, comprising three sub-figures for each column, has been developed. The figure on the left figure shows the numerical curvature data for the three calculation types: NC, aNC, and GM. The central figure depicts the second-order bending moment diagram for the corresponding column, derived from the aNC method. The configuration of this diagram is determined solely by the structural buckling shape. The right figure demonstrates the results of the GM method, which include either the complete bending moment diagram or the axial stress state within the column. This diagram is generated by integrating the stresses of the column member. The analysis of individual column cases revealed a robust concordance with both curvature values and shapes. The second-order bending moment diagram shows a similar configuration using both the aNC and GM methods, reinforcing the postulation that the buckling shape provides a valid assumption for the second-order bending moment distribution.

P-0 and 2P-P cases

The analysis of the two-column frame cases gives interesting results. In the P-0 scenario, two main phenomena can be observed. Firstly, the unloaded column exhibits a second-order bending moment. This is due to the top-level lateral action exerted by the adjacent column, which results in a linear second-order bending moment. It could be argued that the unloaded column provides "support" to the loaded one. Secondly, the interaction between the columns causes an upward shift in the maximum value of the second-order bending moment within the loaded column. This change is confirmed by both the aNC and GM methods. The disparity in curvature for the loaded column is attributed to the primary failure of the unloaded column which occurred in a stress controlled manner. An analogous effect is observed in the 2P-P scenario. However, the difference is that the second-order bending moment is nonlinear due to the simultaneous loading of the other column. The maximum curvature and second-order bending moment for the P-loaded column are located at the base, and this effect shifts upward for the 2P-loaded column.

Fix-hinged and EI case

The fixed-hinged scenario is notable for the requirement that the fixed column must bear the bending moments imparted on both columns. On the contrary, the hinged column is limited to accommodating compressive forces. The application of the aNC method induces a minimal bending moment on this column, due to its inherent buckling configuration. Although this is not essential, it does not introduce any inaccuracies. Similarly, in the EI scenario, the column exhibiting the higher stiffness will bear a larger portion of the loads. It will also assume part of the bending moments of the less rigid column, thereby providing support to this weaker column. This interaction leads to a pronounced upward shift in the curvature and second-order bending moment diagram for the softer column.

5.2 Failure mode

When examining the single-column cases, it is clear that there is no significant difference between the methods in terms of failure modes. In the relatively slender cantilever column scenario, a balanced failure mode was observed, that is, when the concrete reached its ultimate compressive strain, the tensioned bars simultaneously reached their yielding strain. As illustrated in Fig. 6 (left), this represents the maximum bending moment point on the N-M bending interaction diagram.

Regarding the less slender simply supported and fixed-hinged columns, a compression-controlled failure mode was observed, indicating that the tensioned reinforcements remained elastic during the concrete crushing process. The failure modes for each calculation are presented systematically in Table 3. Within NC calculations, due to its focus on isolated columns, an identical failure mode was consistently identified across all calculations, invariably resulting in the failure of the weaker, less stiff, and more heavily loaded column. However, this does not fully encompass the complexities observed in real-world scenarios.

Upon examining the interaction between the columns, certain cases initially yielded unforeseen results. Specifically, when only one of the columns was subjected to loading, it was unexpected to observe the failure of the unloaded column. As the unloaded column was devoid of compression forces, the occurrence of a second-order moment was not anticipated. Nevertheless, due to its connection with the loaded column, second-order moments were indeed present in the unloaded column, as described in Chapter 4.1.

The unloaded column has a reduced bending moment capacity compared to the loaded column. Due to the interaction, second-order bending moments manifest in this column, resulting in a tension-controlled failure mode (see Fig. 7 left). A similar phenomenon is observed when one column bears half the load compared to the other column. This column has a reduced normal force and reduced bending moment capacity compared to the more extensively loaded column. In accordance with the Nominal Curvature method, the second-order bending moment should also be lower. However, due to the interaction with the other column, the second-order bending moment becomes more pronounced for the column with lesser loading, when juxtaposed with calculations performed independently, as delineated in Chapter 4.1. This interaction precipitates a tension-controlled failure in the lesser loaded column prior to the failure of the column subjected to double the load.

When one column is fixed and the other is hinged, only

Table 3: Summary of failure modes

	NC		aNC		GM
Case	Failure mode	Utilization of the other column [%]	Failure mode	Utilisation of the other column [%]	Failure mode
cant	Balanced	-	Balanced	-	Balanced
ss	Compression controlled	-	Compression controlled	-	Compression controlled
bs	Compression controlled	-	Compression controlled	-	Compression-controlled
PP	Balanced	100	Balanced	100	Balanced
P0	Loaded column - balanced	0	Unloaded column - tension controlled	60	Unloaded column - tension controlled
2PP	2P loaded column - balanced	53	P-loaded column - tension controlled	89	2P column - tension controlled
EI	Less stiff column - balanced	26	Stiffer column - tension controlled	44	Buckling
SS	Fix column - balanced	50	Fix column - tension controlled	16	Fix column - tension controlled - buckling

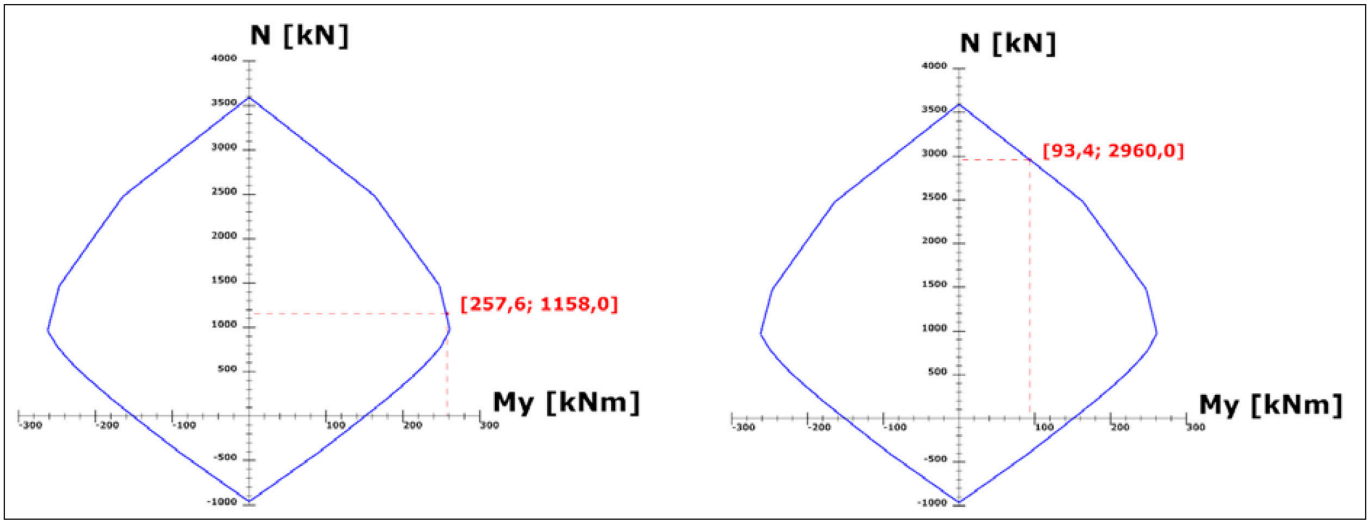

Fig. 6: *N-M bending interaction diagram: for aNC_cant (left) and for aNC_ss (right)*

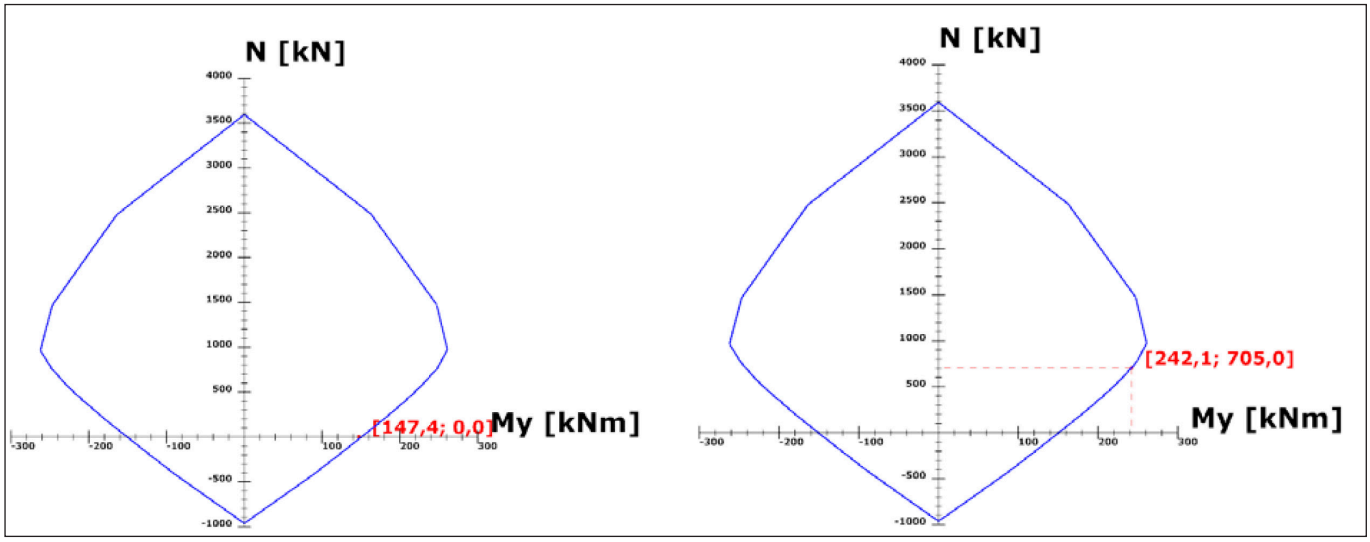

Fig. 7: *N-M bending interaction diagram: for aNC_P0: unloaded column (left), and for aNC_2PP: P loaded column (right).*

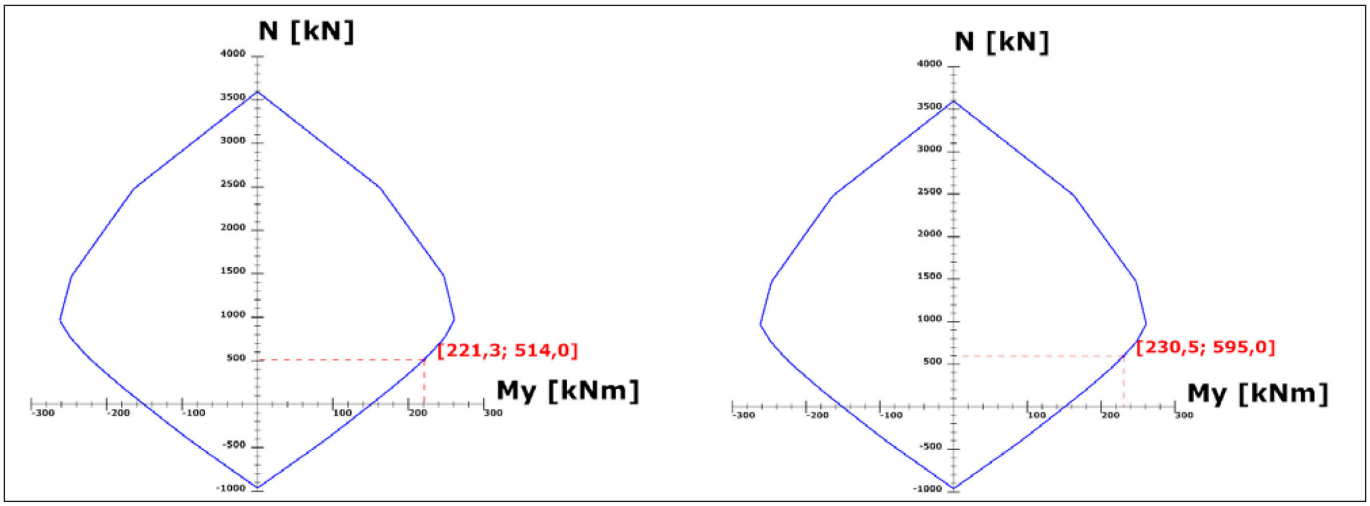

Fig. 8: *N-M bending interaction diagram: for aNC_SS: fixed column (left), and for aNC_EI: stiffer column (right)*

the fixed column will experience bending moments. If the interaction between the columns is not considered, the scenario is similar to a single cantilever column. However, the inclusion of the interaction results in a tension-controlled failure mode that occurs sooner. This is attributed to the fixed column having to withstand the horizontal loads applicable to both columns. As discussed in Chapter 4.1, this results in significantly increased second-order bending moments for the fixed column. A similar phenomenon is observed when the stiffness of one column exceeds that of the other. The Nominal Curvature method predicts the failure of the softer column first. However, with interaction is considered, the stiffer column provides support to the softer column, thereby shifting the failure to the stiffer one due to increased second-order bending moments (see Fig. 8 right).

5.3 Failure load

Table 4 shows the failure loads relevant to the calculations. As explained in Chapters 4.1 and 4.2, there is no significant variation in the calculations for a single column. The

Table 4: Summary of Failure Loads

	GM	NC		aNC	
Case	Failure load [kN]	Failure load [kN]	Difference [%]	Failure load [kN]	Difference [%]
cant	1200	1158	-3,5	1158	-3,5
ss	2885	2960	2,6	2960	2,6
bs	3350	3250	-3,0	3270	-2,4
PP	1200	1158	-3,5	1158	-3,5
P0	1380	1158	-16,1	1300	-5,8
2PP	1635	1158	-29,2	1410	-13,8
EI	667	292	-56,2	595	-10,8
SS	592	1158	95,6	514	-13,2

NC method consistently evaluates isolated elements; consequently, so the failure load of the cantilever column is always 1158 kN. Within the EI model, this load is reduced due to the reduced cross-sectional area. However, the interaction between the columns is completely ignored. In the P-0 and 2P-P scenarios, the failure load is increased in the aNC method and further increased in the GM method, due to the mutual support among the elements. Specifically, in the P-0 context, the unloaded column underpins the loaded one, thus improving its resistance. The increase is limited to 1300 kN, as the unloaded column collapses in a tension-controlled mode. When the alternate column is subjected to half the load, its bending capacity increases, culminating in an increase in the failure load from 1300 kN to 1410 kN in the aNC method and from 1380 kN to 1635 kN in the GM method. In the EI scenario, the failure load increases significantly when the intercolumn interaction is considered, increasing from 292 kN (NC) to 595 kN for the aNC method and to 667 kN for the GM method. Here, the stiffer member provides support to the less rigid column. In all scenarios examined, the interaction resulted in an increased failure load, thereby making the NC method conservative. In contrast, in the SS scenario, the failure load is reduced by half because one column has to support the bending loads of two columns. As the NC method considers an isolated column, this effect is completely overlooked. Although this situation is relatively atypical, it serves as a warning to be more careful when neglecting the interaction between columns.

6. CONCLUSIONS

The role of connected member on the load bearing capacity of compressed reinforced concrete columns was investigated using different calculation methods. Manual calculations were performed according to the nominal curvature method of Eurocode 2, and the automatic nominal curvature method developed in ConSteel was also applied. Furthermore, the general method according to Eurocode 2 was implemented in the ATENA software using nonlinear analysis. To find the differences between the methods, single columns under axial compression with different support conditions were first evaluated, followed by two columns connected by a stiff beam with hinged connections. The columns studied were either loaded at different intensities, had different boundary conditions, or had different cross-sectional areas.

The general method was used as a basis for a more precise consideration of imperfections and geometrical nonlinearity. Our investigation has shown that the nominal curvature method disregards column interaction, which is conservative in most cases. In particular cases, an increase in load on a column, due to the necessity to support substantial loads transferred from other columns, either because one column is more rigid, or because a column is unable to resist horizontal loads, results in the inability of the nominal curvature method to accurately represent the behaviour. This limitation can lead to underdesign and compromise safety. However, the novel approach of the ConSteel software, called the automatic nominal curvature method, which utilises buckling shapes to calculate the distribution of curvatures, was shown to be able to automatically consider the interaction between concrete columns, preventing serious errors from occurring in the case of irregular structural systems.

The effect of creep in this study was taken into account in a simplified manner, further research is needed to better understand its effect on the load bearing capacity of compressed concrete columns. Also the novel method developed in ConSteel should be further studied in order to find more problems where this solution could be applied.

To construct structures that are both safer and more cost-effective, it is essential to account for the interaction among structural elements. Various approaches exist to achieve this, ranging from simplified modelling techniques to the more advanced general method. Ultimately, it is up to the designer's judgement to determine the appropriate solution for the specific problem.

7. ACKNOWLEDGEMENTS

The authors extend their profound gratitude to Professor László Kollár for his invaluable guidance. His conceptual insights on structural analysis were indispensable to this study. Acknowledgements are also due to ConSteel Solutions Kft. for providing a licence, facilitating our exploration of the software's functionalities. We are equally appreciative of Červenka Consulting s.r.o. for their assistance with the general methodology, with particular thanks to Jiří Rymeš for his expertise in meshing and result evaluation.

Project no. BME-380 has been implemented with the support provided by the Ministry of Culture and Innovation of Hungary from the National Research, Development and Innovation Fund, financed under the EKÖP-24-3 funding scheme.

The project was also supported by the Doctoral Excellence Fellowship Programme (DCEP) is funded by the National Research Development and Innovation Fund of the Ministry of Culture and Innovation and the Budapest University of Technology and Economics, under a grant agreement with the National Research, Development and Innovation Office.

8. REFERENCES

EN 1992-1-1-2004. *Eurocode 2: Design of Concrete Structures-Part 1-1: General Rules for Buildings*., 2004

de Araújo, J. M. (2017). „Comparative study of the simplified methods of Eurocode 2 for second-order analysis of slender reinforced concrete columns." *Journal of Building Engineering*, 14, 55–60, Nov. 2017, doi: https://doi.org/10.1016/j.jobe.2017.10.003

Barros, H., Silva, V.D., & Ferreira, C. (2010). „Second-order effects in slender concrete columns-reformulation of the Eurocode 2 method based on nominal curvature." *Engineering Structures*, 32(12), 3989–3993, Dec. 2010, doi: https://doi.org/10.1016/j.engstruct.2010.08.005

Kollár, L.P., Csuka, B., & Ther, T. (2014). „Simplified design of concentrically loaded reinforced concrete columns," *The Structural Engineer: journal of the Institution of Structural Engineer*, 92, 48–56, 2014

Woliński, S. (2011). „Global Safety Factor or Nonlinear Design of Concrete Structures," *Archives of Civil Engineering*, 57, 331-339, Sep. 2011, doi: https://doi.org/10.2478/v.10169-011-0023-3

Cervenka, V. (2013). „Global safety formats in fib Model Code 2010 for design of concrete structures", *Proceedings of the 11th International Probabilistic Workshop,* Brno, 2013

Dobrý, J., Wolfger, H. & Benko, V. (2022). „Reliability of slender concrete columns designed according to the Eurocodes," *Engineering Structures*, 265, 114266, Aug. 2022, doi: https://doi.org/10.1016/j.engstruct.2022.114266

Cervenka, V., Jendele, L., & Cervenka, J. (2020). „Theory," *in ATENA Program Documentation Part 1*, Sep. 2020

Consteel, (2023). „Reinforced concrete columns – applying the Automatic Nominal Curvature Method for design". https://consteelsoftware.com/knowledgebase/reinforced-concrete-columns-applying-the-automatic-nominal-curvature-method-for-design

Szabolcs Szinvai (1997) MSc structural engineer at Budapest University of Technology and Economics. currently pursuing his PhD studies at Department of Structural Engineering, Budapest University of Technology and Economics. Research fields: Embedded FRP reinforcement in concrete structures, focusing on bond and the structural behaviour. A member of the Hungarian group of *fib*, head of the Hungarian *fib* Young Member group and involved in TG10.3 "Examples for Model Code" in *fib*. szinvaiszab@edu.bme.hu

Bálint Vaszilievits-Sömjén (????) Head of R&D Group of Consteel, responsible for the coordination of development of new software features, research tasks. Preparation of webinars and keep international contact with partners involved in Consteel development. balint.vaszilievits-somjen@keszgroup.com

Tamás Kovács (1974) Associate Professor at Budapest University of Technology and Economics, Department of Structural Engineering. Research areas: damage analysis of concrete structures based on dynamic characteristics, high performance concretes for bridges, concrete pavements, reliability of structures. kovacs.tamas@emk.bme.hu

APPENDIX: CURVATURES

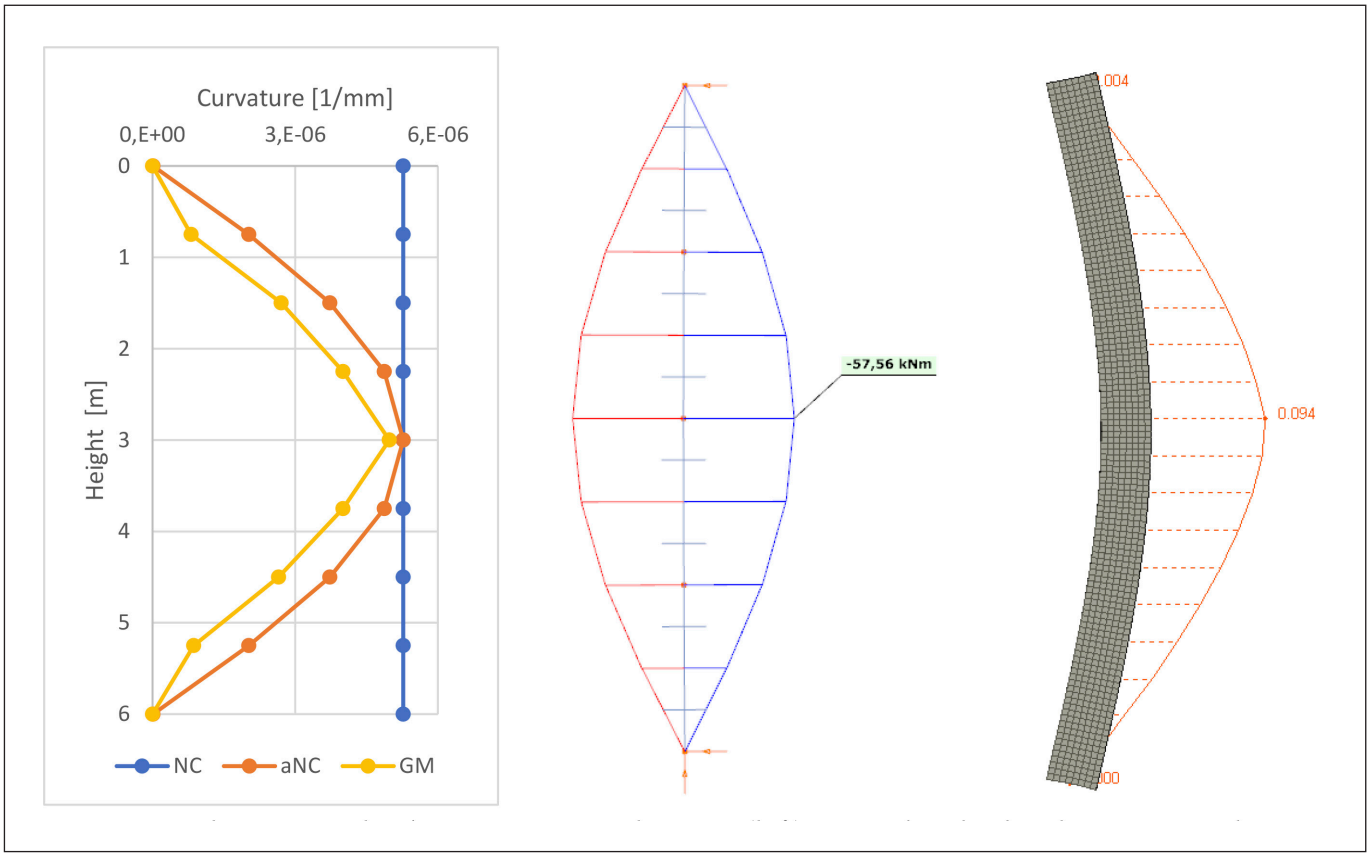

Fig. 9: Simply supported column: curvature diagram (left), second-order bending moment diagram for aNC (middle) and bending moment diagram for GM [MNm] (right)

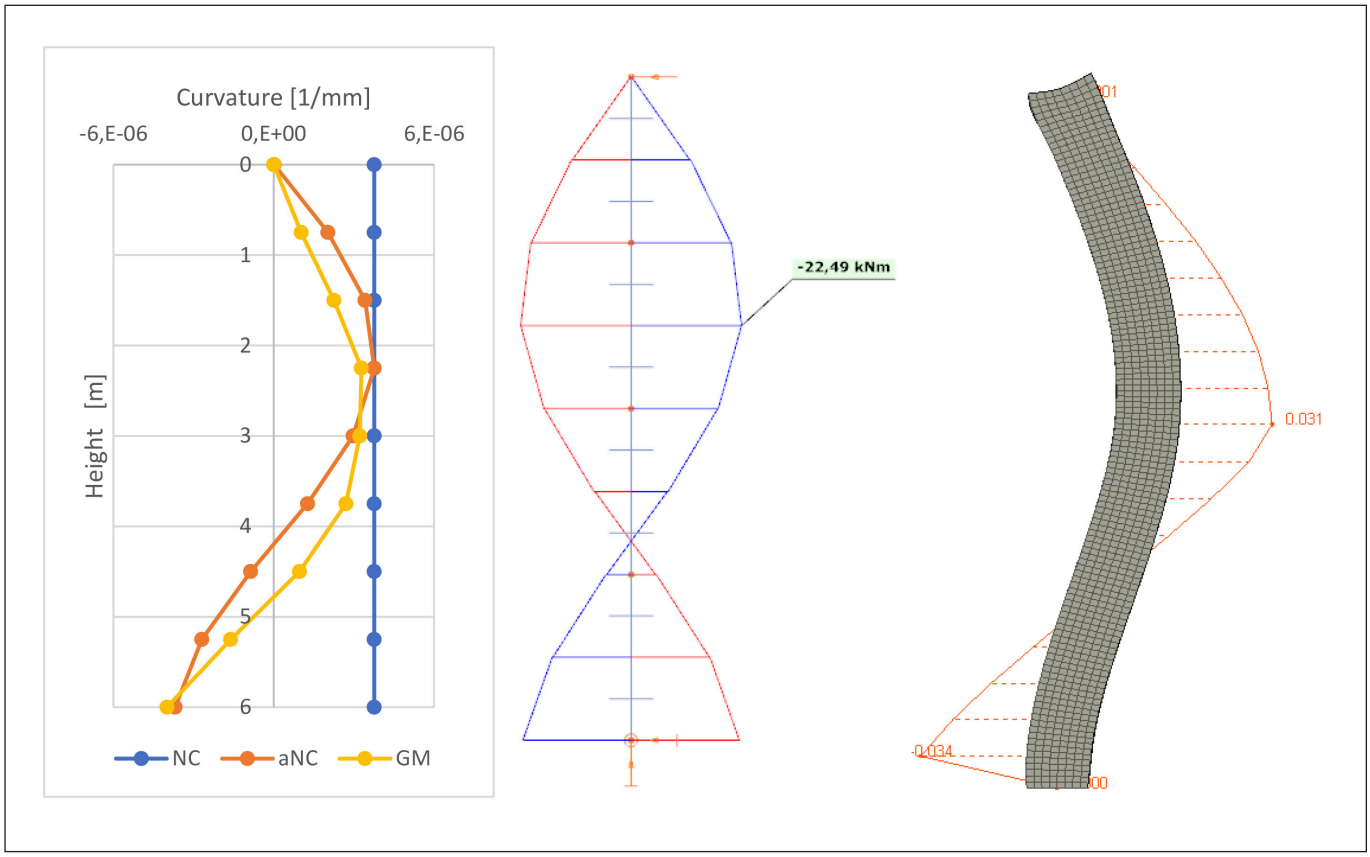

Fig. 10: *Fix-hinged column: curvature diagram (left), second-order bending moment diagram for aNC (middle) and bending moment diagram for GM [MNm] (right)*

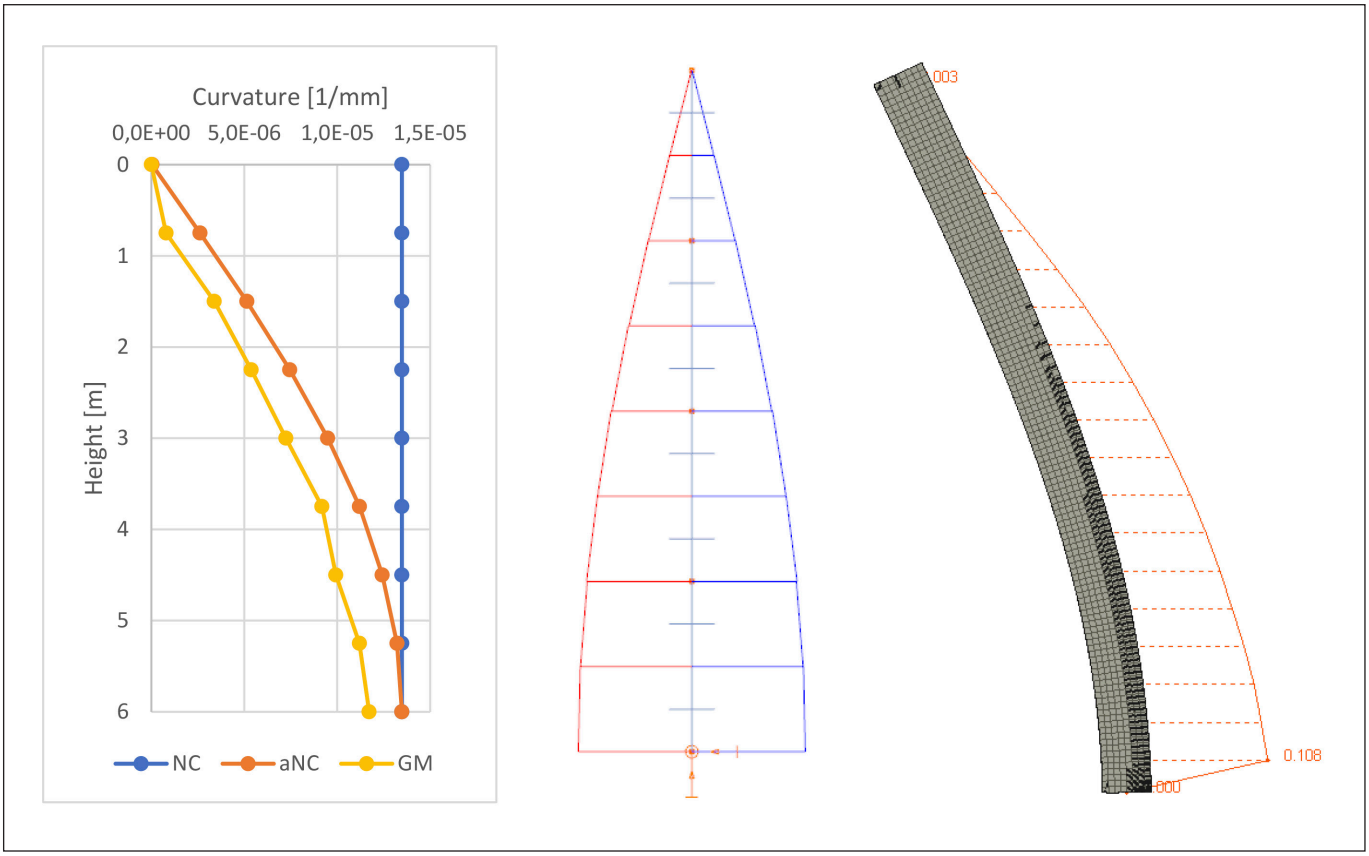

Fig. 11: *Simply supported column: curvature diagram (left), second-order bending moment diagram for aNC (middle) and bending moment diagram for GM [MNm] (right)*

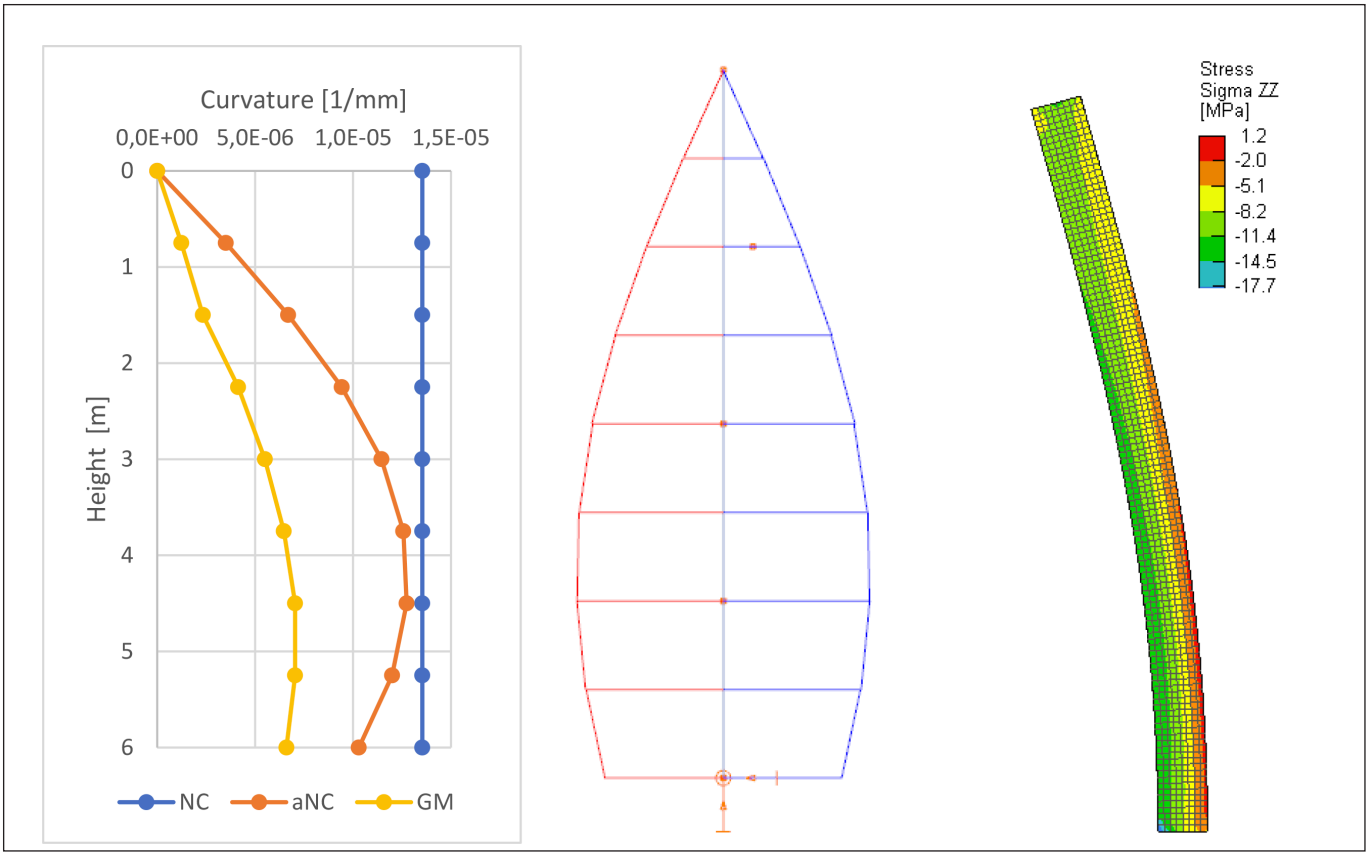

Fig. 12: P-0 case, P loaded column: curvature diagram (left), second-order bending moment diagram for aNC (middle) and stresses for GM [MNm] (right)

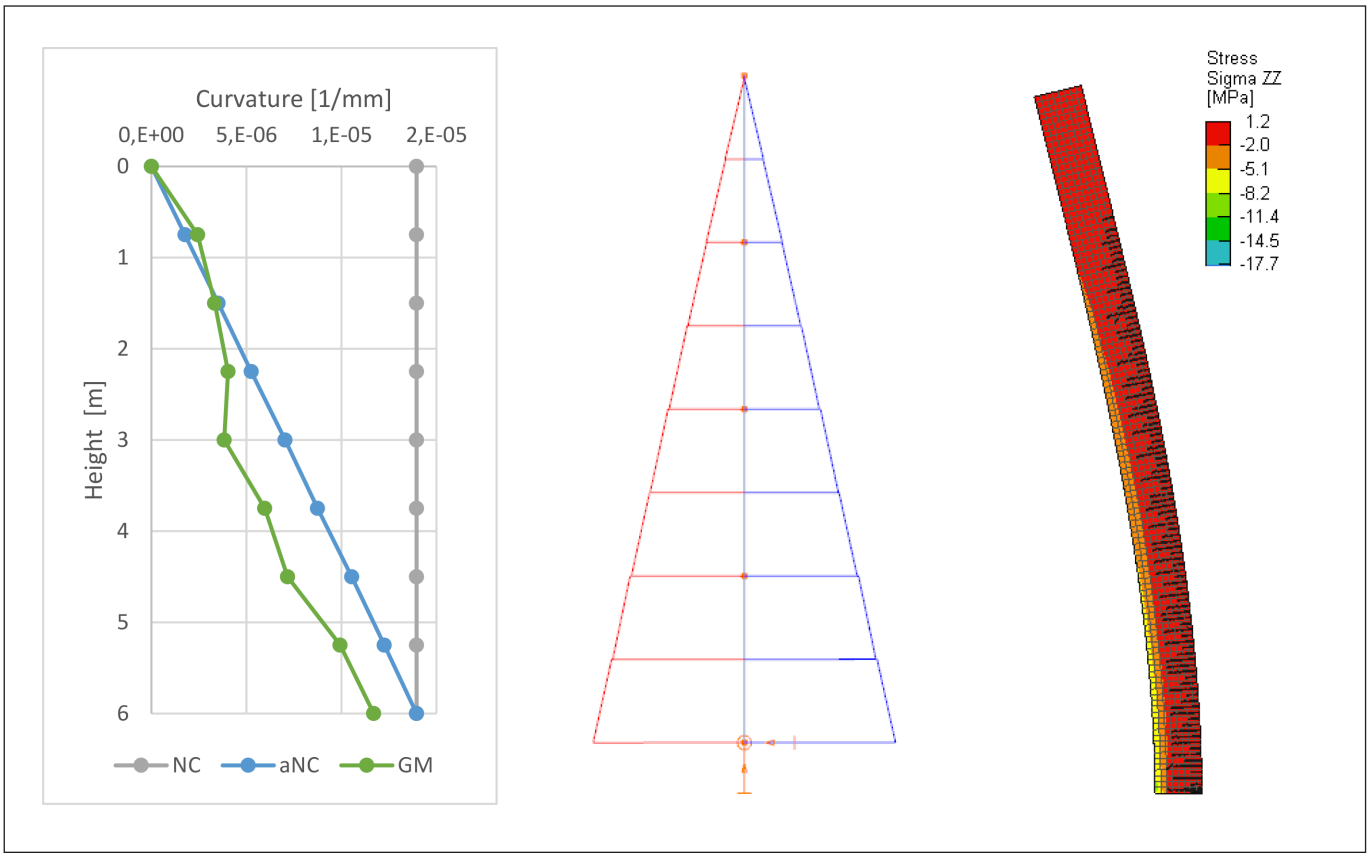

Fig. 13: P-0 case, unloaded column: curvature diagram (left), second-order bending moment diagram for aNC (middle) and stresses for GM [MNm] (right)

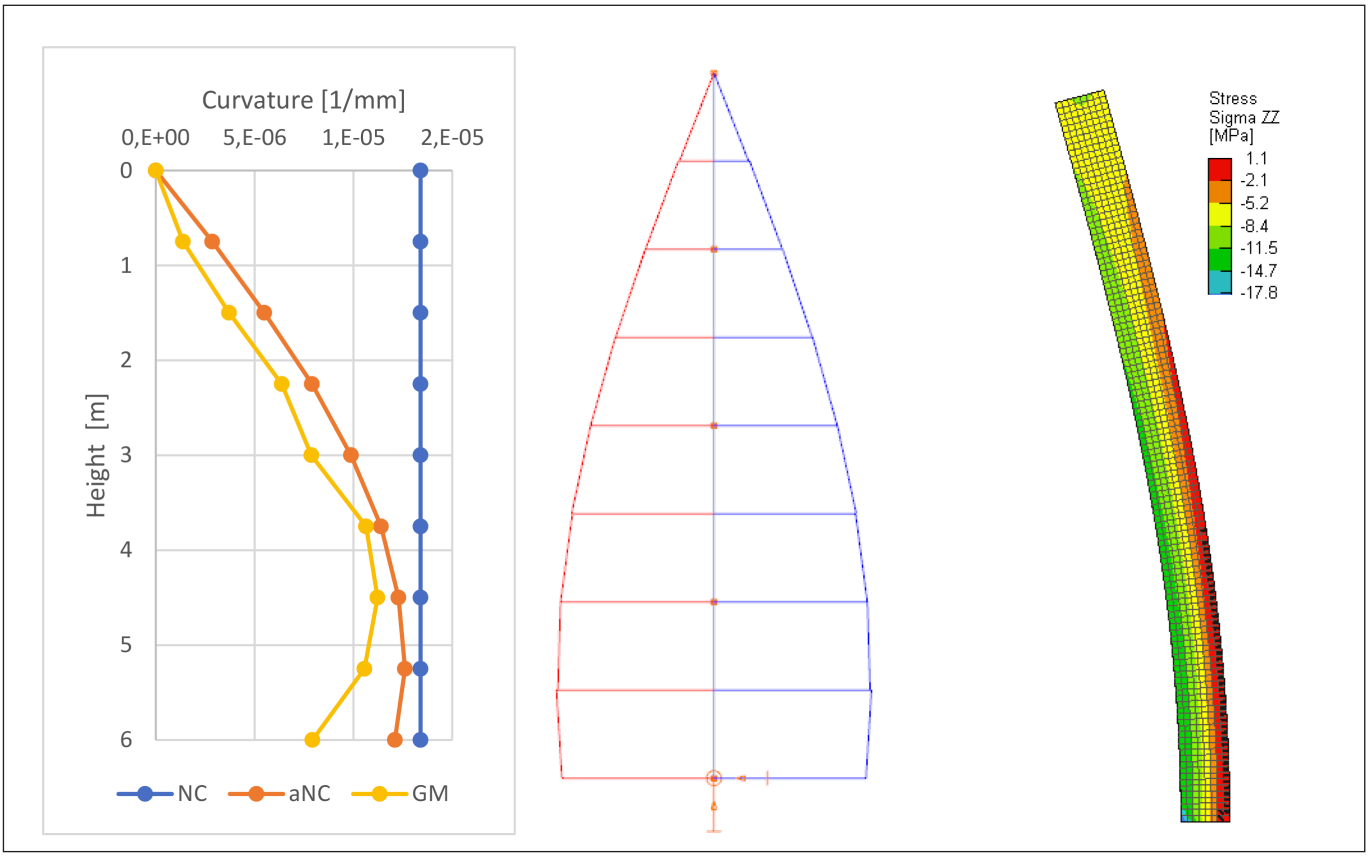

Fig. 14: *2P-P case, 2P loaded column: curvature diagram (left), second-order bending moment diagram for aNC (middle) and stresses for GM [MNm] (right)*

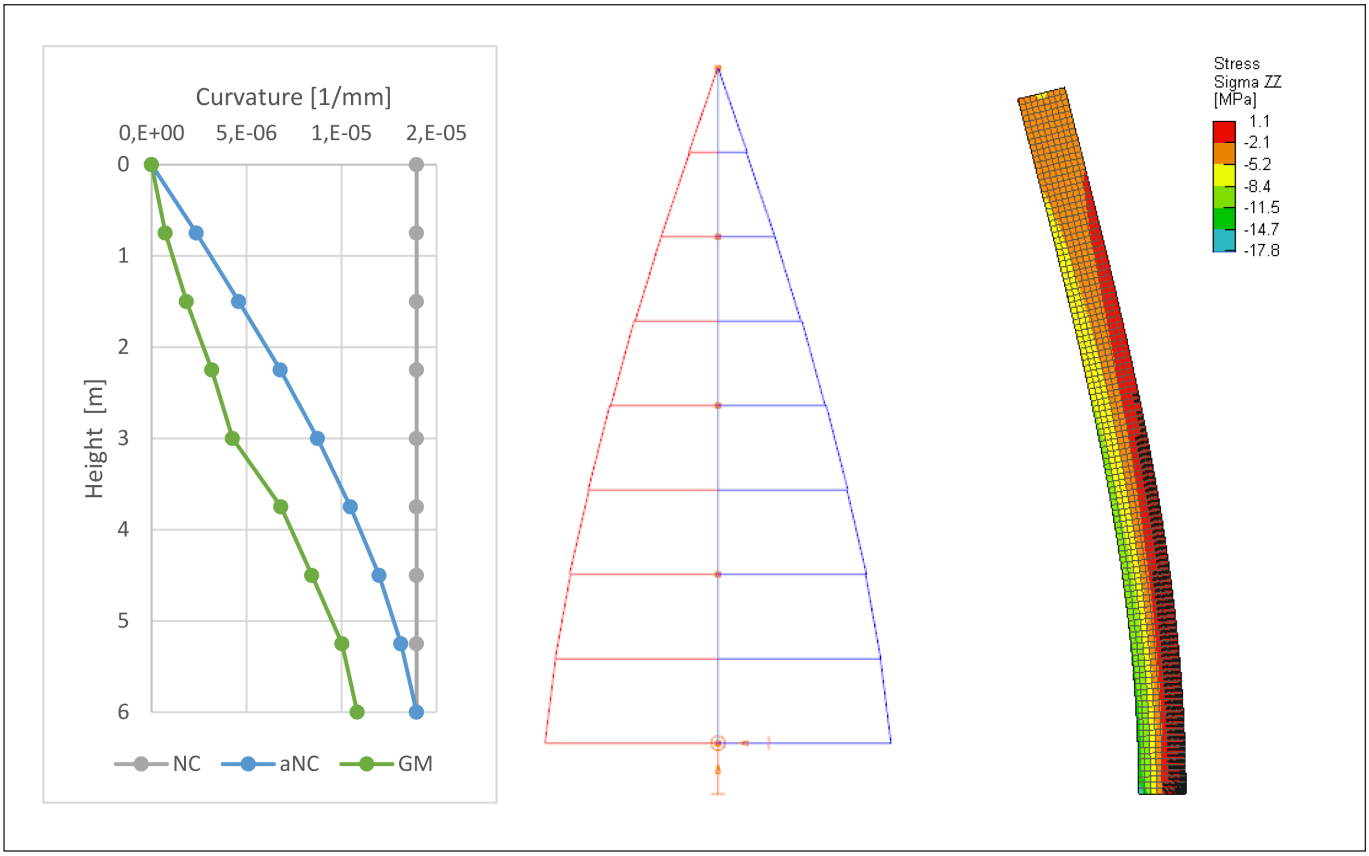

Fig. 15: *2P-P case, P loaded column: curvature diagram (left), second-order bending moment diagram for aNC (middle) and stresses for GM [MNm] (right)*

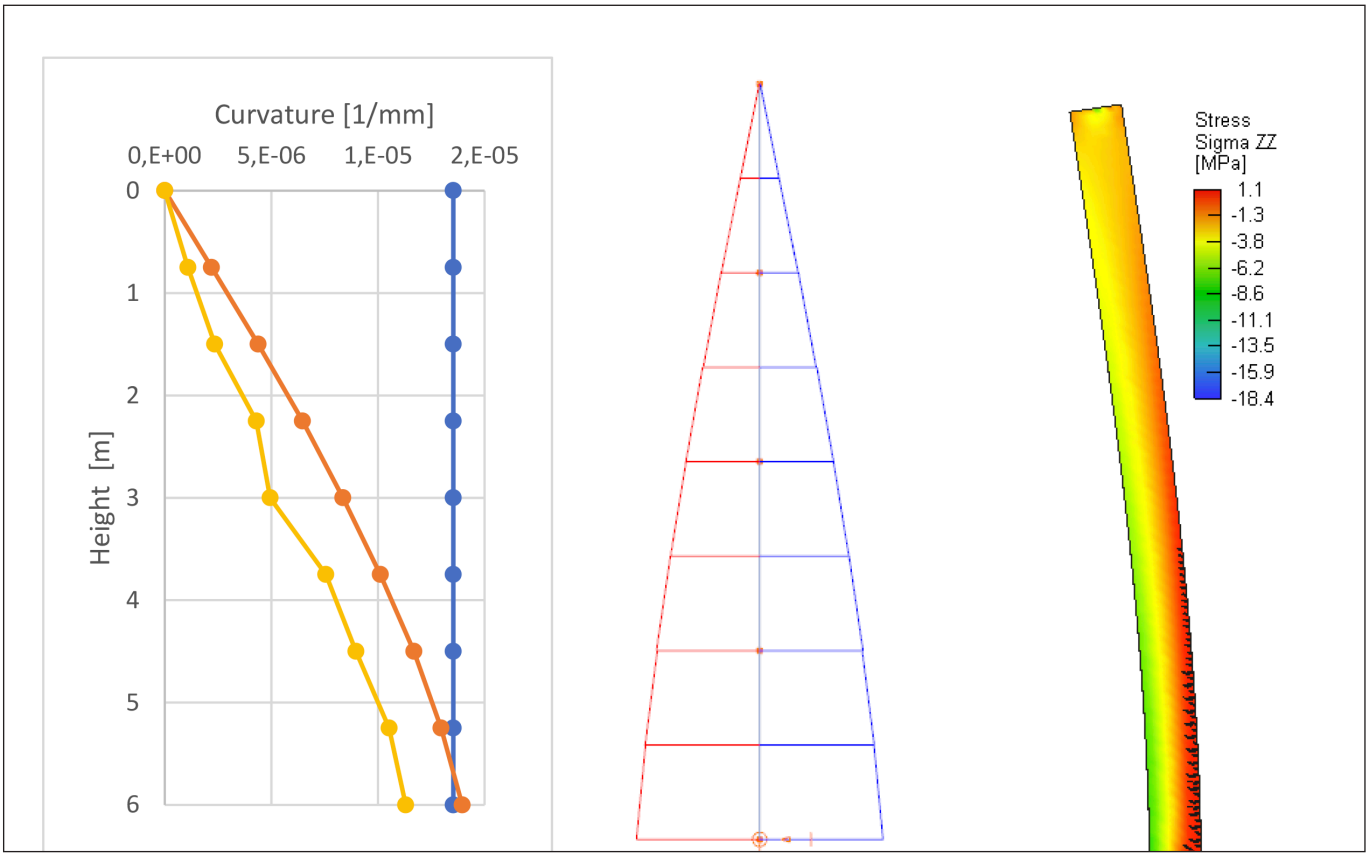

Fig. 16: Fix-hinged, fix column: curvature diagram (left), second-order bending moment diagram for aNC (middle) and stresses for GM [MNm] (right)

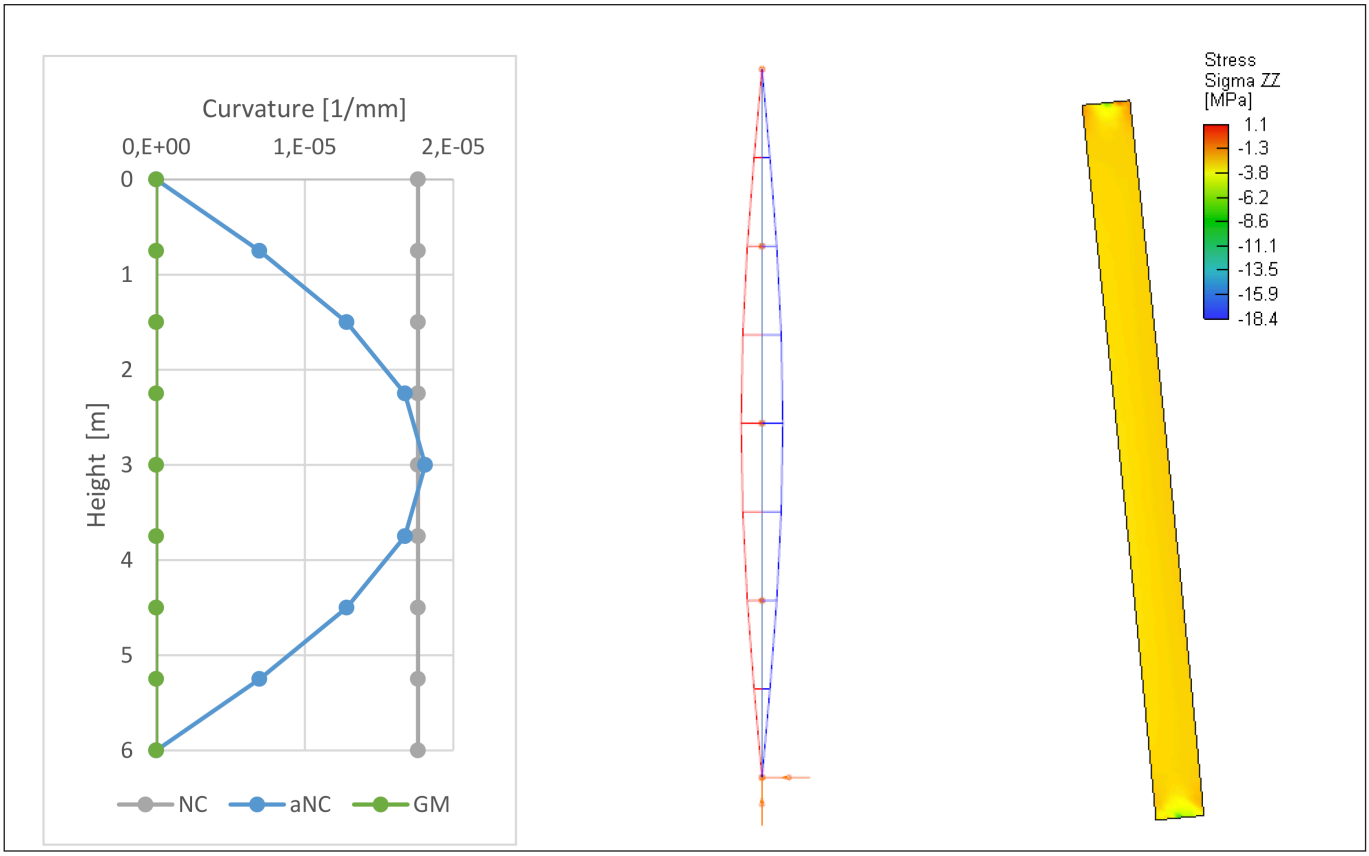

Fig. 17: Fix-hinged, hinged column: curvature diagram (left), second-order bending moment diagram for aNC (middle) and stresses for GM [MNm] (right)

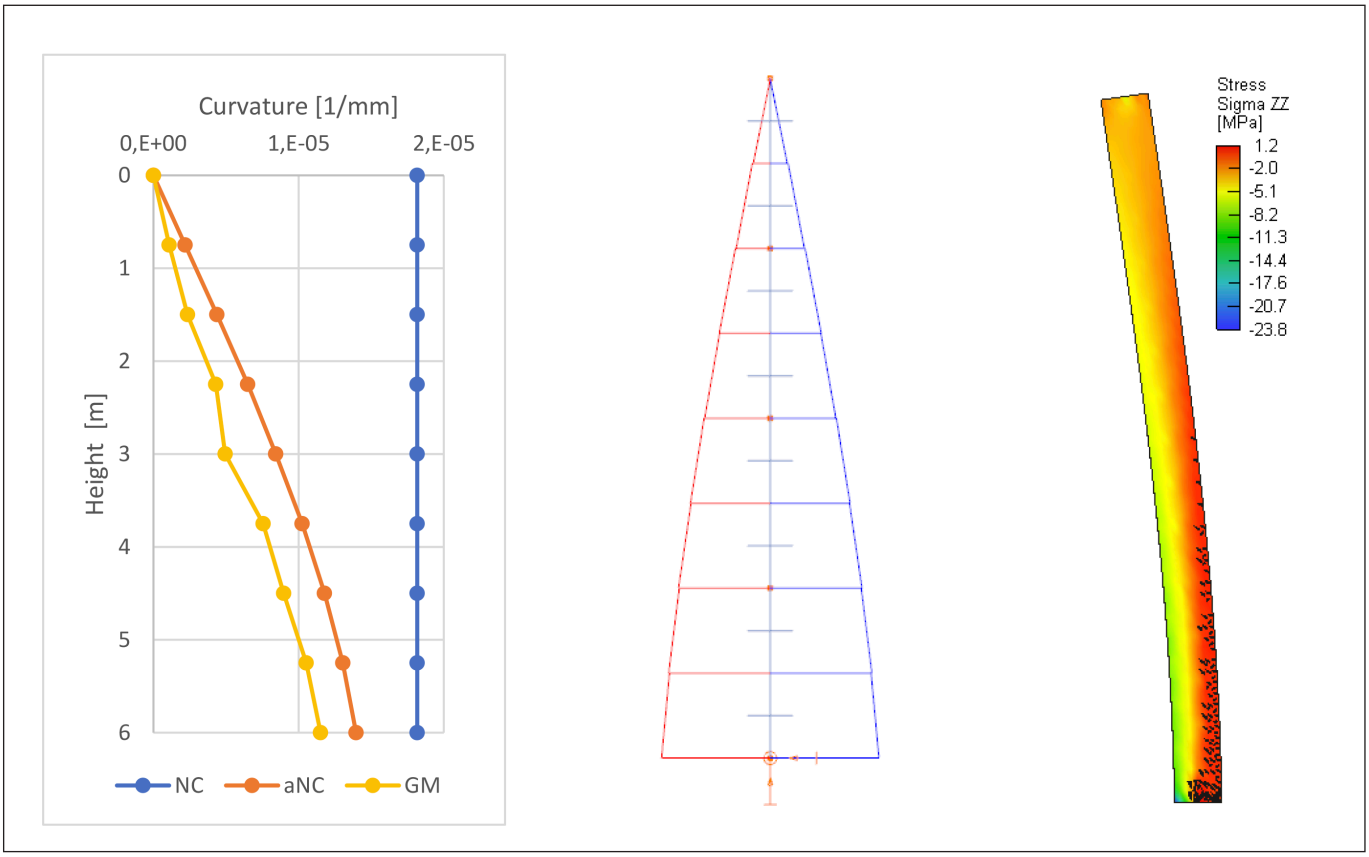

Fig. 18: EI, stiffer column: curvature diagram (left), second-order bending moment diagram for aNC (middle) and stresses for GM [MNm] (right)

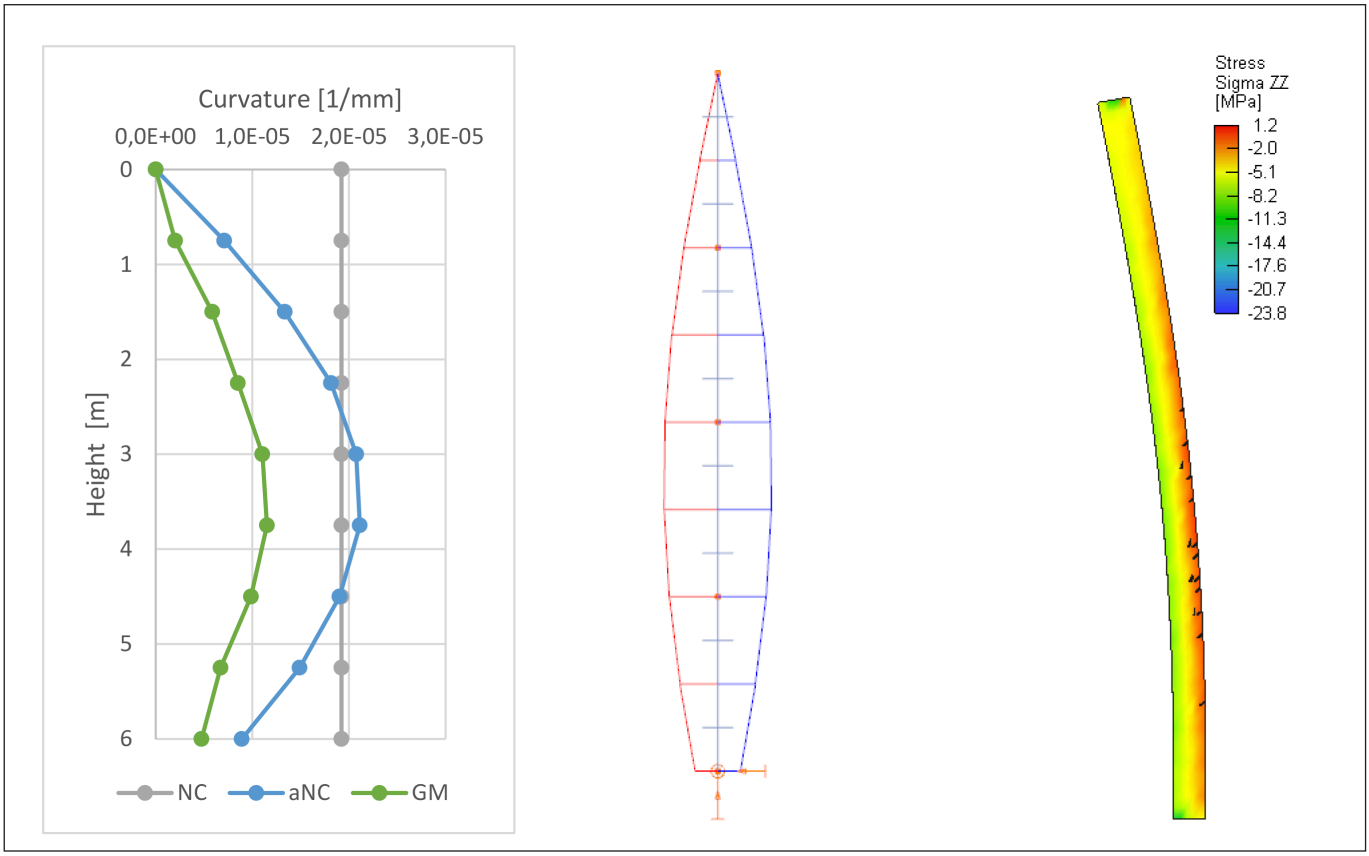

Fig. 19: EI, softer column: curvature diagram (left), second-order bending moment diagram for aNC (middle) and stresses for GM [MNm] (right)

INFLUENCE OF USING STEEL AND POLYPROPYLENE FIBERS ON THE BENDING OF SIFCON


Wisam K. Tuama – György L. Balázs

https://doi.org/10.32970/CS.2024.1.2

Slurry Infiltrated Fiber Concrete (SIFCON) is a special kind of fiber-reinforced concrete that has significant durability and ductility, and it has a higher tensile strength compared to other fiber-reinforced concrete. SIFCON contains a lot of fiber, up to 20% or even more. This study focuses on discovering the effect of two types of fibers, steel and polypropylene, on the bending of SIFCON. A certain number of SIFCON laminates specimens were cast with dimensions of 300×100 mm, with different thicknesses ranging between 10, 20, and 30 mm. Cubes and prisms were also cast to determine the compressive and flexural resistance of the SIFCON concrete for each type of fiber used. After checking all the results, the highest compressive and flexural strength were achieved for SIFCON with steel fiber by 118 and 32.6 MPa respectively, as well as the maximum stress for SIFCON laminates with steel fiber and 30 mm thickness by 16.73 MPa.

Keywords: Slurry Infiltrated Fiber CONcrete, SIFCON laminates, Bending, Steel and Polypropylene fibers

1. INTRODUCTION

Fiber-reinforced cementitious composites (FRCCs) have significantly advanced since the 1970s. It is well acknowledged that FRCC increases the qualities of normal concrete, including tensile strength, stiffness, and fracture resistance. These advantages have encouraged the adoption of FRCC in civil engineering construction. Lankard developed slurry infiltrated fiber concrete (SIFCON), a modification on standard FRCC, in 1984, by putting the steel fiber in mold using huge volumes of it to produce a very dense network of fibers; it is then infiltrated by cement slurry through the network of fibers without employing coarse aggregates in its creation (Lankard R., 1984). The fiber content by volume in SIFCON may vary from 4 to 20%, which is much higher than the typical 2% in conventional fiber-reinforced concrete because of workability and mixing requirements, where the fibers are blended with the other constituents of the concrete: cement, sand, and gravel. Because of its high fiber content, SIFCON has unique mechanical qualities that are superior in ductility, tensile strength, and impact resistance (Fatimah H., and Abeer S., 2020, and Wisam K., György L., 2023).

SIFCON is a steel fiber-reinforced cement composite with exceptional toughness and superior mechanical properties, including compressive, tensile, shear, and flexural strength (Metin I., and Mecbure A., 2019). This new type of special concrete is ideal for explosion-proof military buildings, industrial floors, and bridge piers due to its great toughness and flexural strength (Görkem H., Ferhat A., 2019). The unit weight of SIFCON is high, which exceeds the unit weight of fiber reinforced concrete, because of the high fiber content. The amount of fiber may vary depending on the geometry, aspect ratio, and assignment procedures. If the aspect ratio is reduced, the volume percentage of fibers can be raised. Mild vibrations might also raise the volume fraction. (Ali H., and Nada M., 2022).

The mechanical properties of SIFCON are influenced more by fiber properties such as fiber geometry (shape, length, diameter, and aspect ratio), volume fraction (amount), orientation, fiber type (steel, polymer, elastoplastic, polyolefin, polyethylene, and nylon, or hybrid), tensile strength, and elastic modulus of fibers. Although, the behavior of SIFCON constructed with steel fibers in various shapes, such as straight, hooked end, and crimped (non-straight) fibers, with different aspect ratios, has been documented (Renuka J., and Rajasekhar K., 2021 and Wisam K., György L., 2024).

In this study, the bending of SIFCON laminates specimens containing steel or polypropylene fibers is tested to determine the extent of the effect of using these different types of fibers on SIFCON resistance to bending and recording the maximum load, as well as comparing and discussing the results of the compressive and flexural resistances that were obtained, as well as the difference in SIFCON weight in the two cases.

Review objectives

This paper investigates the properties of slurry infiltrated fiber concrete when using different types of fibers. This study focuses on two main topics: (1) the bending of SIFCON laminates (2) the properties of SIFCON (compressive and flexural strength).

Emphasis is placed on studying how SIFCON bending property is affected by the use steel or polypropylene fibers. Results of this study and summary of how to improve the properties of SIFCON and the bending resistance also discussed.

2. EXPERIMENTAL WORK

2.1 Materials and mix design

In the area of this study, normal quartz sand with 1-4 mm size was used as a fine aggregate. Portland cement type CEM I, and silica fume according to (ASTM C1240, 2020) were used as a binder. Thirty percent used as a water to cementitious materials ratio (w/c), and BASF Master Glenium 300 as a superplasticizer with 1.75 % used in the mix to set adjust consistency of concrete flow (ASTM C494, 2015). In this work, two types of fibers (6%) with different shapes and aspect ratios were used. The first shape was hooked-end steel fibers with a length of 30 mm and a diameter of 0.5 mm. A new type of polypropylene fiber with a length of 25 mm and a diameter of 0.54 mm was also used. *Fig. 1* (a and b) shows the hooked steel fiber and polypropylene fiber used in this research. *Table 1* introduces the technical properties of the two types of fiber used according to the manufacturing company. *Table 2* shows the mixing ratios for SIFCON concrete.

In this experimental work, 6% of the fiber volume fraction was used to achieve the required performance, and a suitable volume of the molds was applied. The procedure of mixing: Blend the dry material for 2 minutes; after that, add 2/3 of water and mix for 3 minutes; leave to rest for 3 minutes. Add the remaining amount of water (1/3) that was mixed with SP and continue mixing for 2 minutes. In this test, the workability of the slurry was achieved with an expansion diameter of 260 mm.

2.2 Test samples

This study included testing of compressive strength and flexural strength of SIFCON and the bending of SIFCON concrete laminates. The compressive strength test was done on 100 mm cubes. The test of flexural strength was done on 40×40×160 mm prisms. The bending tests were performed laminates with 300×100 mm with different thicknesses of 10, 20, and 30 mm.

The results are the average of three cubes or prisms for all sets at the age of 28 days. Also, concrete laminate specimens were examined, and their average was taken. Before casting, the molds of cubes, prisms and laminates were completely cleaned and lubricated. The fiber amount was placed at once before pouring the slurry to penetrate the fibers. To achieve penetration, the mold was lightly knocked with a hand rod. Related to demolding, all samples sank in the basin with water at 25 °C in agreement with (ASTM C192, 2007). *Fig. 2* shows the steps for preparing and lubricating the molds, placing the fibers, pouring the SIFCON concrete, the tamping, and test the different specimens using various examination devices after curing for 28 days.

3. RESULTS AND DISCUSSION

3.1 Mechanical properties

Investigating the compressive strength was done by using a compression testing machine with a loading capacity of 3000 kN at a load rate of 5 kN/s for 100 mm cubes as shown in the pictures in *Fig. 2* and flexural strength of SIFCON concrete was done by using a three-point bend testing machine on a concrete prism. The strength of compressive and flexural at the age of 28 days for the cubes and prisms prepared for this purpose was tested. As a result, the SIFCON reinforced with steel fiber achieved the highest values of 118 and 32.6 MPa

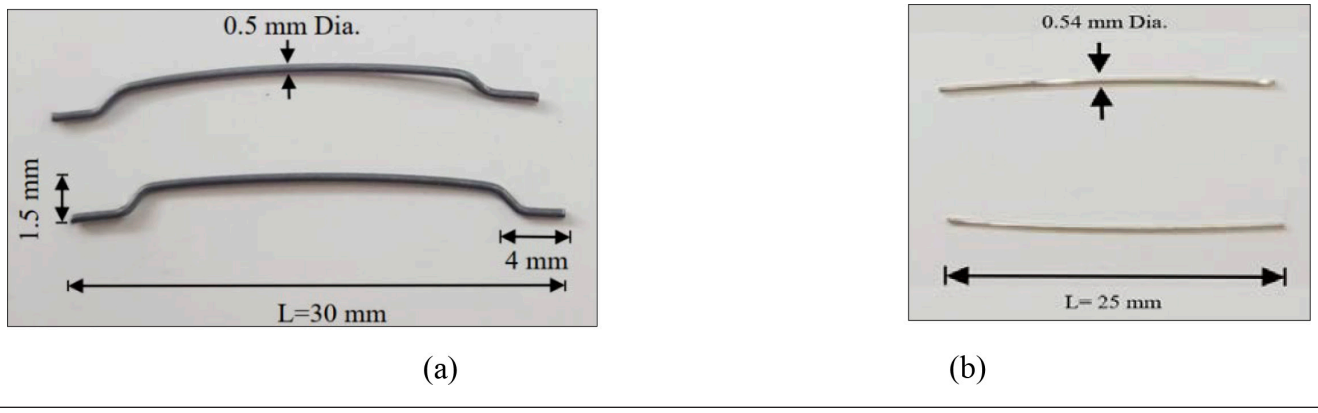

Fig. 1: Types of fiber (a- hooked-end steel fiber and b- polypropylene fiber)

Table 1: Technical properties of the fibers

Fiber type	Length (mm)	Diameter (mm)	Aspect ratio	Density (kg/m^3)	Tensile strength (MPa)
Steel	30	0.5	60	7,850	1,650
polypropylene	25	0.54	46.3	910	490

Table 2: SIFCON optimal mixing proportions for 1 m^3.

Cement (kg/m^3)	Sand (kg/m^3)	Silica Fume kg/m^3 10% rep.	Steel Fiber (%)	w/b or w/c ratio	SP (by wt. of binder) (%)	Slump flow (mm)
873	970	97	6	0.30	1.75	260

Fig. 2: Steps of pouring SIFCON concrete and test the different samples

for compressive and flexural strength respectively. When polypropylene fibers were used, the compressive and flexural strength decreased to 75 and 11.12 MPa respectively. The increase in strength can be explained by the ability of the fibers to restrict and prevent the expansion of the cracks as well as to reduce the growth rate of cracks and change their direction, depending on the characteristics of each type of fiber. This agrees with the researchers (Naser F., Abeer S., 2020, and Ali H., and Nada M., 2022). The reason for the increase in strength is the ability of the steel fiber to expand more than the polypropylene fiber with a greater volume fraction value because it has high tensile strength. It causes a decrease in the amount and the width of the cracks by acting as a bridge for the crack in the sides, which is due to the increasing strength. *Fig. 3* shows the shape of the concrete cube and prism pattern failure according to the use of the fibers and *Fig. 4* shows the compressive and flexural strength results.

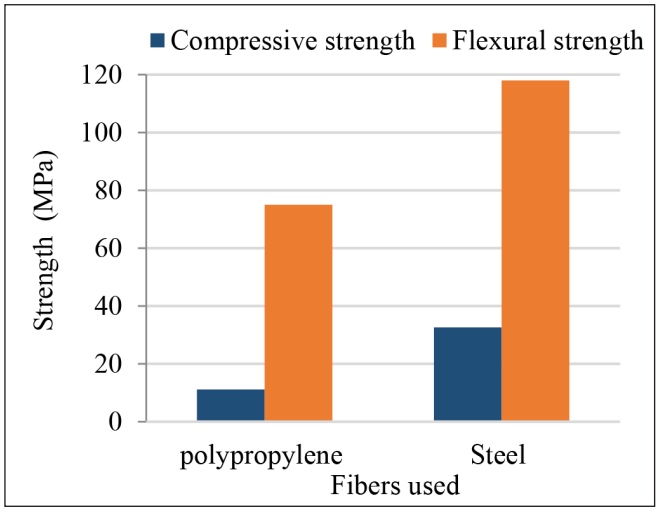

Fig. 4: Results on the compressive and flexural strengths

3.2 Bending of SIFCON

The main objective of this study is to learn the flexural strength of SIFCON concrete and to determine the maximum load that SIFCON laminates can carry. Therefore, SIFCON laminates with dimensions of 300×100 mm with different thicknesses of 10, 20, and 30 mm were cast and tested in a flexural testing device after curing in water for 28 days. The highest load was recorded for SIFCON laminates with the largest thickness of 30 mm when using steel fibers. *Fig.5* shows the maximum stress that can be tolerated by the SIFCON laminates of different thicknesses and according to the type of fibers used.

In the test, the specimens containing steel fibers had higher flexural strength (11.13, 13.47, and 16.73 MPa) than those containing polypropylene (6.92, 8.08, and 9.3 MPa) for laminates with thicknesses 10, 20, and 30 mm respectively. This increase in flexural resistance is considered to be due to the bridging effect of steel fibers in SIFCON, which transfers the stress across cracks more than polypropylene fibers. It was also noted that the difference in the increasing in the maximum load with the increase in the thickness of the specimen is higher when using steel fibers.

Fig. 3: The failure pattern of SIFCON cube and prisms according to the use of fibers (a and c – polypropylene fibers, b and d – steel fibers)

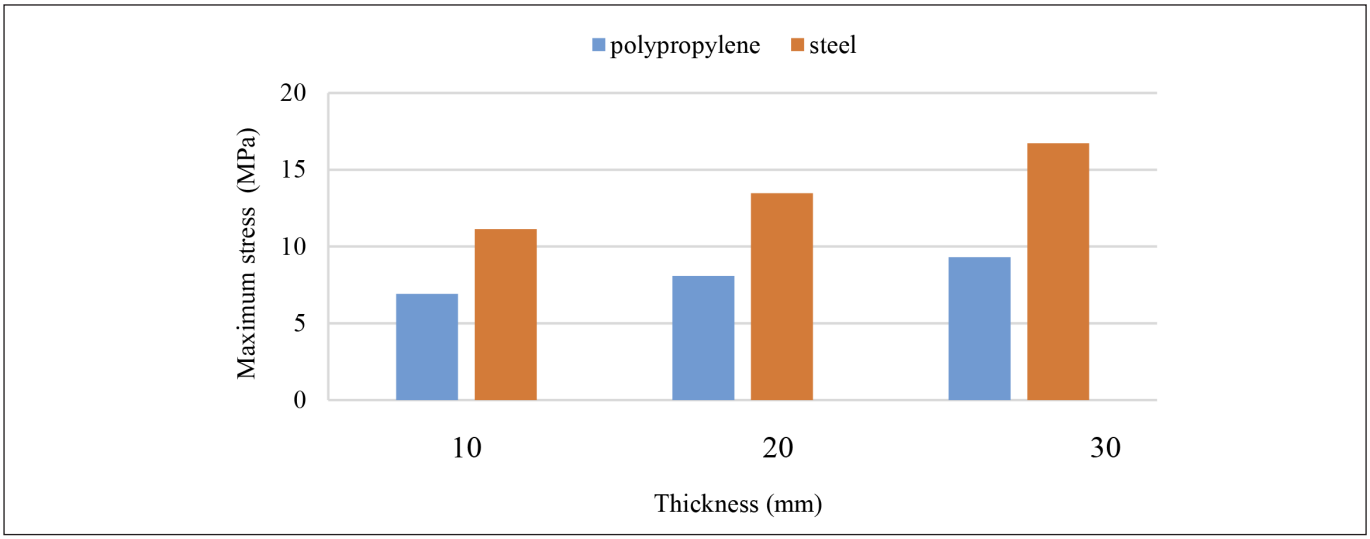

Fig. 5: *The maximum flexural stress of the SIFCON laminates of different thicknesses according to fiber type*

Fig. 6 shows the failure modes for a set of SIFCON laminates. It was observed that both types of fibers were able to obtain the maximum deflection. It was also observed from the results and failure modes that using other types of fibers, such as polypropylene fibers, performs a good function and gives high levels of bending resistance; although they are less than steel fibers, they are characterized by the weight of SIFCON concrete being less than compared to using steel fibers.

4. CONCLUSIONS

The purpose of the current study was to investigate the properties of slurry infiltrated fiber concrete when steel or polypropylene fibers are used (fiber characteristics are given in Fig. 1 and Table 1). This study focuses on investigating the flexural strength of SIFCON laminates and the strength properties of SIFCON (compressive and flexural strength). This study leads to the following conclusions:

1. The use of various fibers (steel and polymeric fibers) in SIFCON concrete makes it suitable for use according to the function that requires the use of this type of concrete, such as high deflection before failure, high energy absorption, and high maximum loads.
2. Among the tested specimens, SIFCON reinforced with steel fibers produced the highest compressive and flexural strength of 118 and 32.6 MPa respectively. When polypropylene fibers were used, the strength fell to 75 and 11.12 MPa for compressive and flexural strength, respectively.
3. The SIFCON laminates reinforced by steel fiber achieved the maximum bending stress of 11.13, 13.47 and 16.73 MPa for 10, 20, and 30 mm thick specimens respectively, and when polypropylene fibers were used, the strength decreased to 6.92, 8.08 and 9.3 MPa in case of 10, 20, and 30 mm thicknesses respectively.
4. It was observed that the SIFCON laminates containing steel fibers with a smaller thickness (10 mm) had higher strength (11.13 MPa) than the SIFCON laminates using polypropylene fibers with a larger thickness of 30 mm where it recorded a strength of 9.3 MPa.

5. ACKNOWLEDGEMENTS

Authors highly acknowledge the MAPEI Ltd. for providing polymeric fibres to the presented tests.

6. REFERENCES

Ali H., and Nada M., (2022). „The effect of using polyolefin fiber on some properties of slurry-infiltrated fibrous concrete.“ Journal of the Mechanical Behavior of Materials, 31, 170–176. https://doi.org/10.1515/jmbm-2022-0020

ASTM 494, (2015). “Standard specification for chemical admixtures for concrete.” West Conshohocken, PA: ASTM International.

ASTM C1240, (2015). “Standard specification for silica fume used in cementitious mixtures.” West-Conshohocken, PA: ASTM International.

ASTM C192 (2007). “Standard practice for making and curing concrete test specimens in the laboratory.” West Conshohocken, PA: ASTM International.

Fatimah H., and Abeer S., (2020). “Flexural behavior of modified weight SIFCON using combination of different types of fibers.” IOP Conf. Series: Materials Science and Engineering 745, 012178. https://doi.org/10.1088/1757-899X/745/1/012178

Görkem H., Ferhat A., (2019). “Examining SIFCON’s mechanical behaviors according to different fiber and matrix phase.” Iranian Journal of Science and Technology, Transactions of Civil Engineering. 43, 501–507.

Fig. 6: *The failure modes of SIFCON laminates (a, b, and c are SIFCON laminates that use polypropylene fiber with 10, 20, and 30 mm thickness respectively, and d, e, and f are SIFCON laminates that use steel fiber with 10, 20, and 30 mm thickness respectively)*

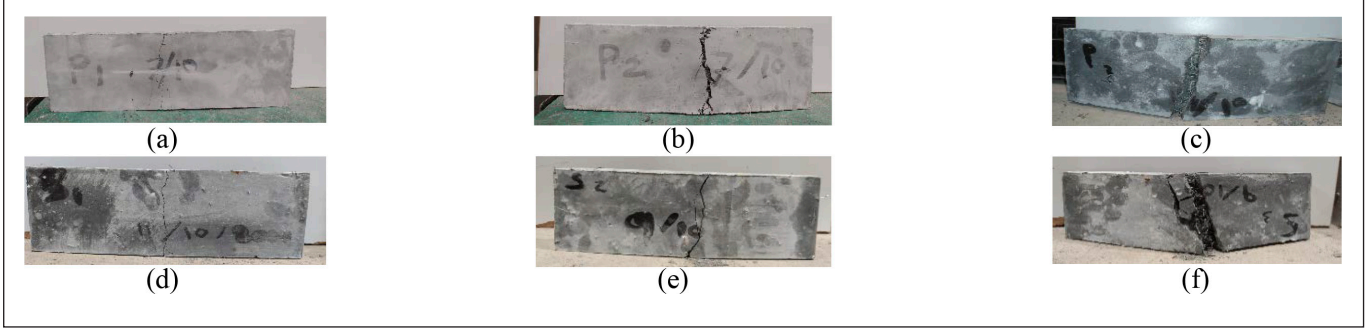

https://doi.org/10.1007/s40996-018-00227-x
Lankard R., (1984). "Properties, applications: Slurry infiltrated fiber concrete (SIFCON)." Concrete International, 6,12, 44–47
Metin I., and Mecbure A., (2019). "The effect of different types of fiber on flexure strength and fracture toughness in SIFCON." Construction and Building Materials. 214, 207–218.
https://doi.org/10.1016/j.conbuildmat.2019.04.055
Naser F., Abeer S., (2020). "Flexural behavior of modified weight SIFCON using combination of different types of fibers." IOP Conf Ser Mater Sci Eng, 745:1.
Renuka J., and Rajasekhar K., (2021). "Performance of Slurry Infiltrated Fibrous Concrete - A Comprehensive Review." Journal of Engineering Science and Technology Review 14(5), 163–172.
https://doi.org/10.25103/jestr.145.19
Wisam K., György L., (2024). "Properties of fibers and mortar of slurry infiltrated fiber concrete (SIFCON)." 14th Central European Congress on Concrete Engineering. ISPN 978-80 908943-1-0, 454–465.
Wisam K., György L., (2023). " Impact and blast resistance of slurry infiltrated fiber concrete (SIFCON): a comprehensive review." Concrete Structures journal, 24, 129–136.
https://doi.org/10.32970/CS.2023.1.18

Wisam K. Tauma (1987), a Ph.D. student at the Department of Construction Materials and Technologies, Budapest University of Technology and Economics (BME). Finished his Bachelor's (2010) in Civil Engineering at the College of Engineering, Thi Qar University in Iraq, and finished his master studies (2019) Master of Science in Construction Materials Engineering at the College of Engineering, Babylon University in Iraq. Research areas: Fiber Reinforced Concrete, durability of concrete, Mechanical Properties of concrete. He is a member of the Hungarian Group of ***fib***.

György L. Balázs (1958), Civil Engineer, PhD, Dr.-habil., Professor of structural engineering at the Department of Construction Materials and Technologies of Budapest University of Technology and Economics (BME). His main fields of activities are experimental investigation and modeling of RC, PC, FRC, FRP, HSC, HPC, LWC, fire resistance and fire design, durability, sustainability, bond and cracking. He is chairman of several commissions and task groups of ***fib***. He is president of Hungarian Group of ***fib***, Editor-in-chief of the Journal "Concrete Structures". He was elected as President of ***fib*** for the period of 2011-2012. Since then, he is Honorary President of ***fib***. Chairman of ***fib*** Com 9 Dissemination of knowledge.

A REVIEW OF EXPERIMENTAL FACTORS INFLUENCING BOND STRENGTH AT ELEVATED TEMPERATURES


Ahmed Omer Hassan Ali – Éva Lublóy

https://doi.org/10.32970/CS.2024.1.3

After a fire, engineers must determine if a building should be demolished or repaired based on its condition and ability to support future loads. Evaluating the structure's strength post-fire is essential. High temperatures can degrade concrete properties—such as compressive and tensile strength, and the bond between rebar and concrete. These properties are vital for assessing the building's safety and design. Evaluating bond strength at elevated temperatures is complex, as the heating procedure, heating rate, and cooling process influence the bond after exposure to fire. Although researchers recognize these factors, the extent of their impact remains a topic of debate. After a fire, researchers typically evaluate residual bond strength using pullout and beam tests to assess material deterioration. This measurement is expressed as the ratio of bond strength at high temperatures (ranging from 20 °C to 800 °C) to the bond strength at ambient temperature, which is usually around 20 °C.

This paper reviews the literature on bond strength at elevated temperatures, investigating the factors that affect this strength. It discusses the bond-slip curve and the impact of different experimental variables, including the heating procedure, rate and duration, cooling method, rebar properties, specimen characteristics, and the residual bond strength following high-temperature exposure.

Keywords: bond, elevated temperature, pull-out test, beam test, residual bond strength

1. INTRODUCTION

The bond between rebar (reinforcing steel) and concrete refers to the adhesion and mechanical interlock between the two materials, which allow force transfer between the two materials. This mechanism enables reinforced concrete to act as composite materials to resist applied loads. As a result of this bond, the forces in the steel and concrete change along the length of the rebar, leading to different strains in the two materials and causing relative displacement, known as slip (*fib* Bulletin No. 10, 2000). This mechanism ensures satisfactory structural performance of concrete elements, allowing for ductile failure with adequate warning (Morley, and Royles, 1980).

Factors influencing bond strength are known under normal conditions, but measuring their effects remains a topic of ongoing research. Material characteristics—like concrete strength, aggregate type, and admixtures—along with testing methods significantly affect bond strength performance (ACI Committee 408,2003; Diederichs and Schneider, 1981). At high temperatures, the physical properties of concrete change significantly (Abuhishmeh etal.,2024), which weakens the bond between the concrete and the reinforcing rebar (Lublóy and Hlavička, 2017), affecting the structural behavior and compromising the overall structural integrity.

This review paper examines the effects of elevated temperatures on the bond between rebar and concrete, exploring the bond degradation and studying the factors that impact bond strength under thermal stress. Understanding this behavior ensures buildings' safety and durability in extreme thermal conditions.

2. CHARACTERIZING BOND-SLIP BEHAVIOR AT ELEVATED TEMPERATURES

Bond test samples can fail in two ways: pullout failure and splitting failure, unless the rebar fails. The *fib* model code 2010 represents these modes in *Figure 1* as the bond-slip curve, summarized in the following equations.:

$$\tau_b = \tau_{bmax}\left(\frac{s}{s_1}\right)^{\propto} \; for\; 0 \le s \le s_1 \quad (1)$$

$$\tau_b = \tau_{b\,max}\; for\; s_1 < s \le s_2 \quad (2)$$

$$\tau_b = \tau_{b\,max} - \left(\tau_{bmax} - \tau_{bf}\right)\left(\frac{s-s_2}{s_3-s_2}\right) \quad for\; s_2 \le s \le s_3 \quad (3)$$

$$\tau_b = \tau_{bf}\; for\; s_3 \le s \quad (4)$$

where

τ_{bmax} = *maximum bond stress*

s = slip

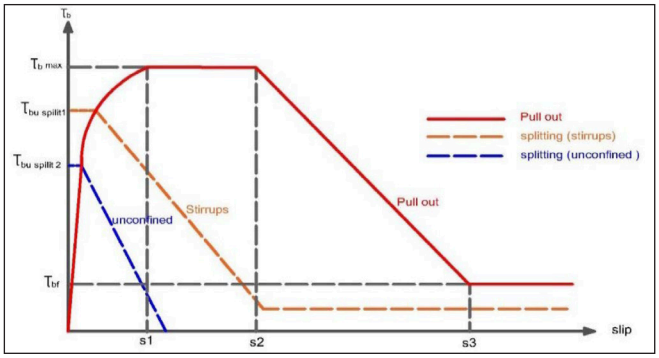

Figure 1: Fib model for Bond-Slip curve (The fib Model Code 2010).

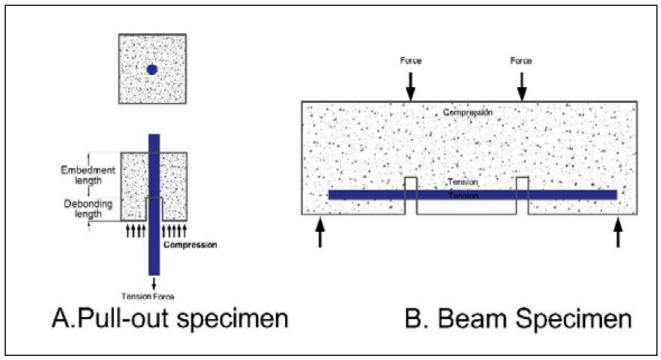

Figure 2: Shapes of specimens for bond strength testing.

The bond strength deteriorates at elevated temperatures, leading to a flattening and nonlinearity of the bond stress-slip curve. Scholars have suggested modifications to the *fib* bond-slip model (*fib* Model Code, 2010) to account for the effects of temperature, such as those proposed by (Lublóy and Hlavička, 2017) and (Aslan and Samali, 2013); these modifications are shown in *Table (1)*. These modifications involve revised formulas for the local bond stress–slip relationship, which depends on the temperature to which the specimen is exposed, the type of aggregate, and the concrete's strength classification (high or low).

3. EFFECT OF EXPERIMENTAL VARIABLES ON BOND STRENGTH UNDER HIGH TEMPERATURES

3.1. Characteristics of the Specimen

Research commonly divides Bond strength specimens into two main categories: direct pullout and beam tests (Zheng etal., 2023), as shown in *Figure 2*. Typically, pullout test specimens are either prisms or cylinders. Several studies (Sharmaa etal., 2019; Muciaccia and Consiglio, 2021; Banoth and Agarwal, 2020; Lublóy and Hlavička, 2017) have investigated pullout specimens under elevated temperatures, while other researchers have used beam specimens for bond tests such as (Ghazaly etal., 2018; Xiao etal., 2014; Ghajari and Yousefpour, 2023; Bošnjak etal., 2018) , with preference in terms of behavior to beam specimens, as it replicates stress conditions found in actual structures in contrast to pullout tests (Das etal., 2023). In a pullout test, the concrete is subjected to compression, while the rebar experiences tension; however, in actual structures, both components are in tension. This difference results in variations in the bond strength evaluation under both normal and elevated temperatures, which limits the practical applicability of models based on pullout tests. Therefore, it is essential to establish correlations between pullout test results and structural performance (Cairns and

Table 1: Modified fib Model Parameters at Elevated Temperatures

Variables	Lublóy and Hlavička, 2017					Aslan and Samali, 2013	
Aggregate type	quartz confined		quartz and expanded clay confined			-	-
Type of concrete	HSC		HSC			HSC	NSC
Temperature range °C	20 -400	400 - 800	20 -500	500 - 700	>800	100-800	
s_1 mm	1.00		1.00			0.5	1
s_2 mm	3.00		3.00			2	3
s_3 mm	CR		CR			CR	CR
$\propto$	0.4		0.4			$\propto$	$\propto$
$\tau_{b\,\max}$	$2.5f_{ck}^{0.5}$	$f_{ck}^{0.4}$	$2.0f_{ck}^{0.5}$	$f_{ck}^{0.4}$	0	$\frac{\tau_{b\,\max.T}}{\tau_{b\,20}} = 1.0538\left(\frac{f'_{cT}}{f'_{c}}\right) - 0.0255 \quad 30\,mm < l_b \leq 100$ f'_{cT} has diiferent equations for HSC and NSC $\tau_{b\,\max.T}$ varies for different embedment lengths (l_b).	
τ_{bf}	$f_{ck}^{0.5}$	-	$f_{ck}^{0.5}$	-	-	$0.4\tau_{b\,\max.T}$	$0.4\tau_{b\,\max.T}$

Remark: CR: clear distance spacing between ribs

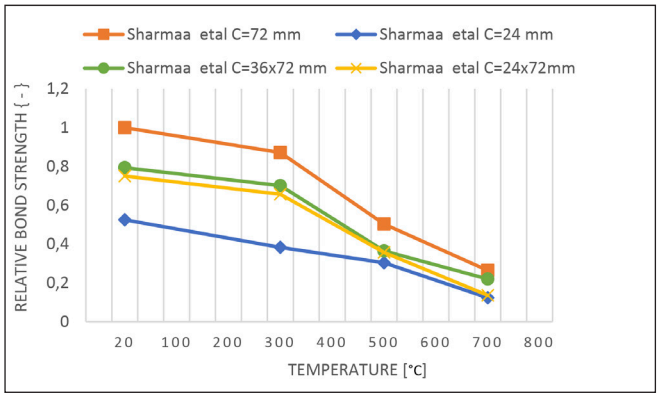

Figure 3: Residual bond strength (Sharmaa et al. to reference bond strength with c=72) as a function of temperature

Abdullah, 1995). Furthermore, new studies are needed to analyze bond behavior in beam specimens.

3.2. Influence of concrete cover on bond strength specimens

Experiments conducted on concrete specimens with varying cover sizes at different temperatures show that larger concrete covers are more likely to fail through pull-out. This failure happens because the concrete in direct contact with the rib experiences compressive stress; in contrast, specimens with smaller concrete covers tend to fail due to tensile splitting (Sharmaa etal., 2019; Muciaccia and Consiglio, 2021; Morley and Royles, 1983).

The study by (Sharmaa etal., 2019) , which is depicted in *Figure 3,* demonstrates that both maximum and minimum cover sizes of prism samples significantly impact bond strength. Larger cover sizes result in higher bond strength; this effect is maintained at both ambient and elevated temperatures. However, the bond strength enhancement due to larger cover becomes less pronounced at higher temperatures, particularly at 500 °C and 700 °C. Because the strength and stiffness of the concrete decline with temperature increases.

3.3 Influence of rebar properties on bond strength at elevated temperature

Diederichs and Schneider (1981) investigated the influence of bar surface properties using plain rebar and two types of deformed bars; the tests showed a significant deterioration in bond strength for the specimens. Also, the tests they conducted, as well as tests by (Ergün etal., 2016), demonstrated that deformed rebars exhibited temperature-bond relationships like those of plain rebars. However, in both studies, deformed rebars performed better than plain rebars, as illustrated in *Figure 4*. (Hertz, 1982) investigated how bar diameter affects bond strength degradation in pull-out specimens subjected to elevated temperatures. The conclusion was that when the temperature rose to 500 °C, the diameter of the rebar had a relatively small impact on the degradation of bond strength. A recent study by (Muciaccia and Consiglio, 2021) examined samples with four and eight-diameter embedment lengths using a constant force method. The findings revealed no significant difference in bond strength for specimens featuring centered bars. The difference occurred when the rebar was positioned at the edge or side and diminished when evaluating bond strength as a function of temperature .

Figure 4: Influence of rebar rib characteristics on residual bond strength at elevated temperature

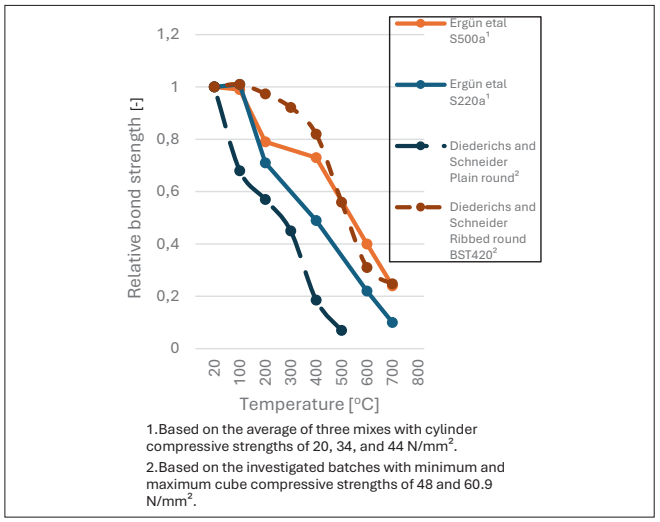

3.4 Impact of thermal treatment on bond strength

Bond strength is influenced by the testing procedures used. To evaluate the effect of temperature on bond strength, as shown in *Figure 5,* researchers typically use two primary methods: the stabilized temperature procedure and the constant load procedure (Diederichs and Schneider, 1981; Muciaccia and Consiglio, 2021). The stabilized temperature procedure includes different stress scenarios based on whether the specimen is stressed during heating and its temperature state (hot or cold) during testing, leading to four unique testing scenarios with different impacts on bond strength, as shown in *Figure 5;* Morley and Royle's tested the four conditions shown in *Figure (6)*, the result indicate that specimens subjected to stress during the heating cycle demonstrate slightly greater strength than those not stressed (Royles and Morley, 1983). This increased strength is primarily attributed to the confinement provided by the loading. In the constant load procedure, specimens are continuously loaded while heated until failure occurs. The constant load procedure is essential for evaluating a structure's capacity to bear its weight during a fire (Muciaccia and Consiglio, 2021). Muciaccia and Consiglio analyzed the two procedures; again, the findings revealed that the reduction in bond strength is more pronounced during the constant load procedure (Muciaccia and Consiglio, 2021).

A rapid rate or slow heating rate can be adopted depending on experiment requirements; the rapid rate can be adopted using the ISO standard fire curve to simulate the behavior of fire in practice (ISO 843, 2019); also, a slow rate can be used in the experiment; this will eliminate the resulting stress from the different movement between the hot outer surface and the colder core of the specimen, and as a result, this test procedure will isolate and demonstrate the effect of temperature on bond strength alone (Morley and Royles, 1980).

(Banoth and Agarwal, 2020) measured bond strength using two methods: one with a slow heating rate of 2 °C/min and another with a fast-heating rate, following the standard of ISO 834 to reach the required temperature. There was a substantial decrease in bond strength for the samples that were heated faster. This indicates that faster heating rates result in quicker bond strength degradation as shown in *Figure 7.* Lee et al. found similar results in samples tested by

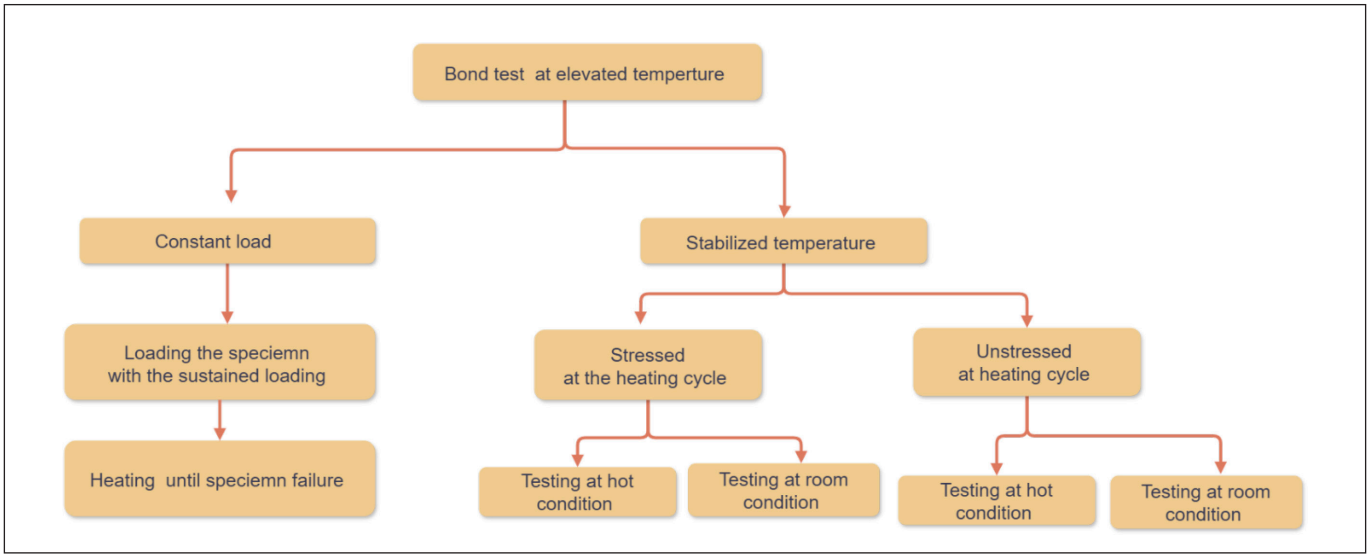

Figure 5: *Experimental Procedure for Bond Testing at Elevated Temperatures*

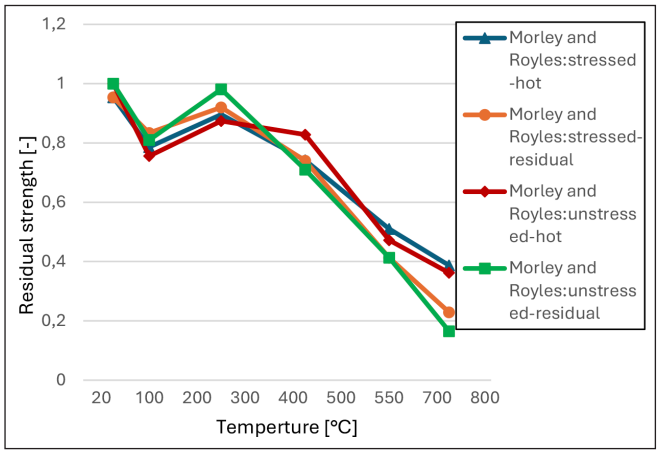

Figure 6: *Bond Strength Response to Heat Using Stabilized Method (Morley and Royles, 1980)*

applying 2 °C/min and 15 °C/min; Lee et al. also found that the cooling method using water or air did not significantly impact the bond strength of samples with uncoated rebar (Lee et al., 2018).

3.5 Residual bond strength of concrete after high thermal exposure

Generally, the failure mode will determine whether bond strength depends on compressive or tensile strength (*fib* Bulletin No. 72 , 2014). Research conducted by (Morley and Royles, 1983) and (Lublóy and Hlavička, 2017) found that the effect of temperature on bond strength is more pronounced than its effect on compressive strength.

Figure 8 shows the residual bond strength results from tests by (Lublóy and Hlavička, 2017) and (Morley and Royles, 1983). The bond strength decreased with increasing temperature, about 30% deterioration up to 200 °C. At 600 °C, considered critical for the structural integrity of Portland cement concrete, deterioration ranged from 65% to 90%, primarily due to the decomposition of calcium hydroxide around 450 °C. Additionally, mixes containing expanded clay and quartz gravel, tested by Lublóy and Hlavicka, experienced a more significant bond strength reduction beyond 150 °C.

Sharma et al. suggested a linear relationship derived from test results, which conservatively exhibits the reduction in relative bond strength of normal-strength concrete at high temperatures (Sharmaa et al 2019). The following equation

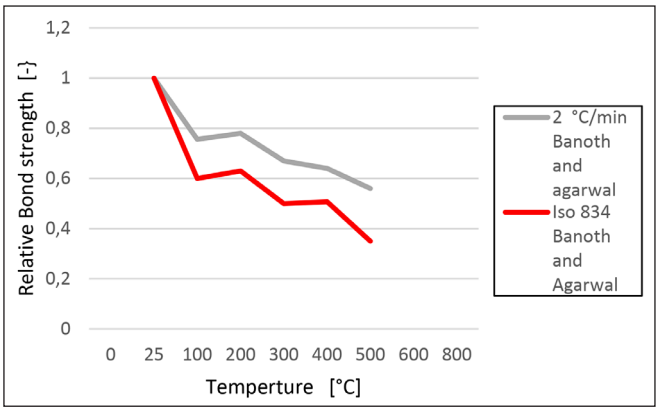

Figure 7: *Heating Rate vs. Residual Bond Strength according to (Banoth and Agarwal, 2024)*

represents the model:

$$\tau_{buT} = \tau_{bu,20}\left(1 - \frac{T-20}{780}\right) \quad (5)$$

where:

T_{buT} is the residual strength at T (°C)

$T_{bu,20}$ is the bond strength at (20 °C) using the *fib* Model Code 2010 equation.

Additionally, (Ergün et al , 2016) introduced mathematical equations that focus on the impact of rebar properties, considering different steel grades (S220a, S420a, S500a). The following equation represents the model:

For S220a T>200 0C

$$S_T = \left[0.618X\left(\left(\frac{T}{1000}\right)^2\right) - 1.681X\left(\frac{T}{1000}\right) + 1.036\right] X\ RBS_{(T=20^oC)} (R = 0.99) \quad (6)$$

For S420a T>200 ^{0}C

$$S_T = \left[-0.821X\left(\left(\frac{T}{1000}\right)^2\right) - 0.0268X\left(\frac{T}{1000}\right) + 1.023\right] X\ RBS_{(T=20^oC)}\ (R = 0.98) \quad (7)$$

For S500a T>200^{0}C

$$S_T = \left[-0.629X\left(\frac{T}{1000}\right)^2 - 0.352X\left(\frac{T}{1000}\right) + 0.905\right] X\ RBS_{(T=20^oC)}\ (R = 0.96) \quad (8)$$

ere

temperature in ^{0}C

$S_{(T=20\ ^0C)}$ is the residual at 20 ^{0}C.

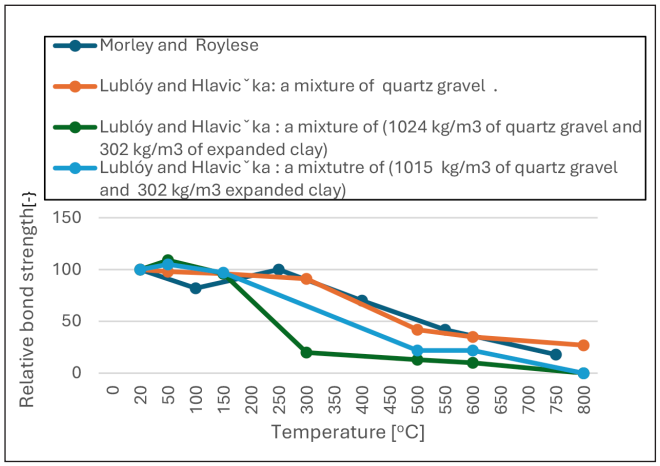

Figure 8: Residual relative bond strength at different temperatures for different concrete mixes

Haddad et al. prepared specimens using plain concrete and concrete reinforced with fibers, incorporating three different types of fibers to create various mixes. Below 600 °C, adding fibers enhanced the residual bond strength by helping prevent crack propagation and spalling. The highest residual bond performance was observed in the concrete mix containing only Hooked Steel fibers (Haddad et al, 2008).

4. CONCLUSIONS

This work reviews the available literature on bond strength at elevated temperatures, including factors such as testing methods and empirical models. It can be concluded from the scientific papers included in this literature review that:

1. Most studies utilized pull-out specimens; therefore, further research is needed to link pull-out behavior to actual structures.
2. Additional research is necessary, mainly through beam tests, to comprehend the actual mechanisms influencing residual bond strength at elevated temperatures.
3. Researchers use various methods in their experiments, such as stabilized temperature and constant load procedures. While much of the current research focuses on the constant temperature method and its impact on residual bond strength, there is an increasing demand for studies that compare this method with the constant load procedure. Existing studies indicate that the reduction in bond strength is more significant under the constant load procedure.
4. A larger cover results in greater bond strength at both ambient and elevated temperatures; however, the decrease in residual bond strength with temperature is similar after 500 °C.
5. The heating rate is a crucial factor because faster rates of heating lead to more rapid degradation of bond strength
6. Cooling using air or water does not influence the residual bond strength of uncoated rebar.
7. Mild and deformed rebars show similar residual bond strength curves, but plain rebars deteriorate more quickly.
8. The diameter of the rebar has little to no effect on the residual bond strength.
9. The concrete mix composition, including aggregate type, pozzolanic content, and fiber type and amount, affects residual bond strength. Further research using beam specimens and different heating methods is needed to explore these factors, along with the development of more models to predict bond strength at elevated temperatures.

5. REFERENCES

Abuhishmeh, K., Jalali, H. H., Ebrahimi, M., Soltanianfard, M., Cesar Ortiz Correa, J. S. (2024), „Behavior of high strength reinforcing steel rebars after high temperature exposure: Tensile properties and bond behavior using pull-out and end beam tests", *Engineering Structures*, 305, https://doi.org/10.1016/j.engstruct.2024.117730

ACI committee 408 (2003), „ Bond and Development of Straight Reinforcing Bars in Tension", ACI 408R-03.

Aslan, A.,Samali, B. (2013), „Predicting the bond between concrete and reinforcing steel at elevated temperatures", *Structural Engineering and Mechanics*, 48(5),pp. 643-660, https://doi.org/10.12989/sem.2013.48.5.643

Banoth, I., Agarwal, A. (2020), „Effect of Heating Rate on Bond Behavior Between Steel and Concrete at Elevated Temperatures". *Advances in Structural Engineering*, 74, pp. 89-98,https://doi.org/10.1007/978-981-15-4079-0_8

Banoth, I., Agarwal, A. (2024), „Bond between deformed steel rebars and concrete at elevated temperatures", *Fire Safety Journal,* 145, https://doi.org/10.1016/j.firesaf.2024.104133

Bošnjak, J., Sharma, A., Öttl, C. (2018), „ Modified beam-end test setup to study the bond behavior after fire", *Materials and Structures*, 51, https://doi.org/10.1617/s11527-018-1138-7

Cairns, J,Abdullah, R. (1995), „ an evaluation of bond pullout test and their relevance to structural performance", *The Structural Engineer*, 73(11).

Das, A., Bonšjak, J., Sharma, A. (2023), „ Post-fire bond behaviour of reinforcement in concrete considering different bonded lengths and position of rebars", *Engineering Structures*, 296, https://doi.org/10.1016/j.engstruct.2023.116908

Diederichs, U., Schneider, U. (1981), „Bond strength at high temperatures", *Magazine of Concrete Research*, 33(115),pp.75-84,https://doi.org/10.1680/macr.1981.33.115.75

Ergün, A., Kürklü, G., Baspınar, M. S. (2016), „The effects of material properties on bond strength between reinforcing bar and concrete exposed to high temperature", *Construction and Building Materials*, 112,pp. 691–698. http://dx.doi.org/10.1016/j.conbuildmat.2016.02.213

fib Bulletin No. 10 (2000), „ Bond of reinforcement in concrete", https://doi.org/10.35789/fib.BULL.0010

fib Bulletin No. 72 (2014), „Bond and anchorage of embedded reinforcement: background to the fib Model code 2010", https://doi.org/10.35789/fib.BULL.0072

Ghajari, F. A., Yousefpour, H. (2023), „Residual bond-slip behavior in reinforced concrete members exposed to elevated temperatures", *Structural Concrete*, 24, pp. 3281–3298, https://doi.org/10.1002/suco.202200927

Ghazaly, N., Rashad, A., Kohail, M., Nawawy, O. (2018), „Evaluation of bond strength between steel rebars and concrete for heat damaged and repaired beam-end specimens", *Engineering Structures*, 175, pp.661–668, https://doi.org/10.1016/j.engstruct.2018.08.056

Haddad, R., Alsaleh, R., Al-Akhras, N. (2008), „Effect of elevated temperature on bond between steel reinforcement and fiber reinforced concrete", *Fire Safety Journal*, 43(5), pp. 334–343, https://doi.org/10.1016/j.firesaf.2007.11.002

Hertz, K. (1982), „ The anchorage capacity of reinforcing bars at normal and high temperatures". *Magazine of Concrete Research*, 34(121), pp.213-22, https://doi.org/10.1680/macr.1982.34.121.213

ISO 834 (2019), „ Fire-resistance tests - Elements of building construction".

Lee, J., Sheesley, E., Jing, Y., Xi, Y., Willam, K. (2018), „The effect of heating and cooling on the bond strength between concrete and steel reinforcement bars with and without epoxy coating", *Construction and Building Materials*, 177, pp.230–236. https://doi.org/10.1016/j.conbuildmat.2018.05.128

Lublóy, É., Hlavička, V. (2017), „Bond after fire", Construction and Building Materials, 132, pp.210-218. http://dx.doi.org/10.1016/j.conbuildmat.2016.11.131

Morley, P. D., Royles, R. (1980), „ The Influence of High Temperature on the Bond in Reinforced Concrete". *Fire Safety Journa*l, 2,pp. 243 - 255. https://doi.org/10.1016/0379-7112(79)90024-9

Morley, P. D., Royles, R. (1983), „ Response of the bond in reinforced concrete to high temperatures”, *Magazine of Concrete Research*, 35(123),pp. 67-74,https://doi.org/10.1680/macr.1983.35.123.67

MSZ EN 1991-1-2. (2002), „ Actions on structures – Part 1–2: General actions – Actions on structures exposed to fire”.

Muciaccia, G., Consiglio, A. N. (2021), „Local bond properties of reinforcement in concrete subjected to elevated: Effects of clear cover, bonded length and heating and loading procedure”, *Engineering Structures*, 230, https://doi.org/10.1016/j.engstruct.2020.111594

Royles, R., Morley, P. D. (1983), „ Further responses of the bond in reinforced concrete to high temperatures”, *Magazine of Concrete Research*, 35(124), pp.157-163, https://doi.org/10.1680/macr.1983.35.124.157

Sharmaa, A., Bošnjakb, J., & Bessertc, S. (2019), „ Experimental investigations on residual bond performance in concrete subjected to elevated temperature”. *Engineering Structures*, 187, pp.384-395, https://doi.org/10.1016/j.engstruct.2019.02.061

The *fib* Model Code (2010), „The fib Model Code for Concrete Structures 2010”.

Xiao, J., Hou, Y., & Huang, Z. (2014), „ Beam test on bond behavior between high-grade rebar and high-strength concrete after elevated temperatures”, *Fire Safety Journal*, 69, pp.23-35. https://doi.org/10.1016/j.firesaf.2014.07.001

Zheng ,Y., Fan, C., Ma, J., Wang, S.(2023), „Review of research on Bond–Slip of reinforced concrete structures”, *Construction and Building Materials*, 385, https://doi.org/10.1016/j.conbuildmat.2023.131437

Ahmed Omer Hassan Ali

Ahmed Omer Hassan Ali, MSc in Structural Engineering and a PhD candidate at the Budapest University of Technology and Economics. He is a Graduate Member of the Institution of Structural Engineers (IStructE) with research interests in fire resistance, progressive collapse, and the bond behavior between reinforcement and concrete. With experience as a Structural Engineer and Lecturer.

Department of Construction Materials and Technologies, Faculty of Civil Engineering, Budapest University of Technology and Economics, Műegyetem rkp. 3., H-1111 Budapest, Hungary.

Éva Lublóy

Dr. Éva Lublóy (1976) civil engineer (2002), concrete technology engineer (2010), fire protection designer (2011), doctor of Hungarian Academy of Sciences (2022), professor at the Department of Building Materials and High Pressure Treatment, BME (2022). Main fields of interest: behaviour of reinforced concrete structures under fire, fire damage engineering lessons learned, non-destructive diagnostic methods for materials. Member of the ***fib*** Hungarian Section.

15TH PHD SYMPOSIUM IN CIVIL ENGINEERING 2024 BUDAPEST
PARTICIPATING UNIVERSITIES (69 UNIVERSITIES)

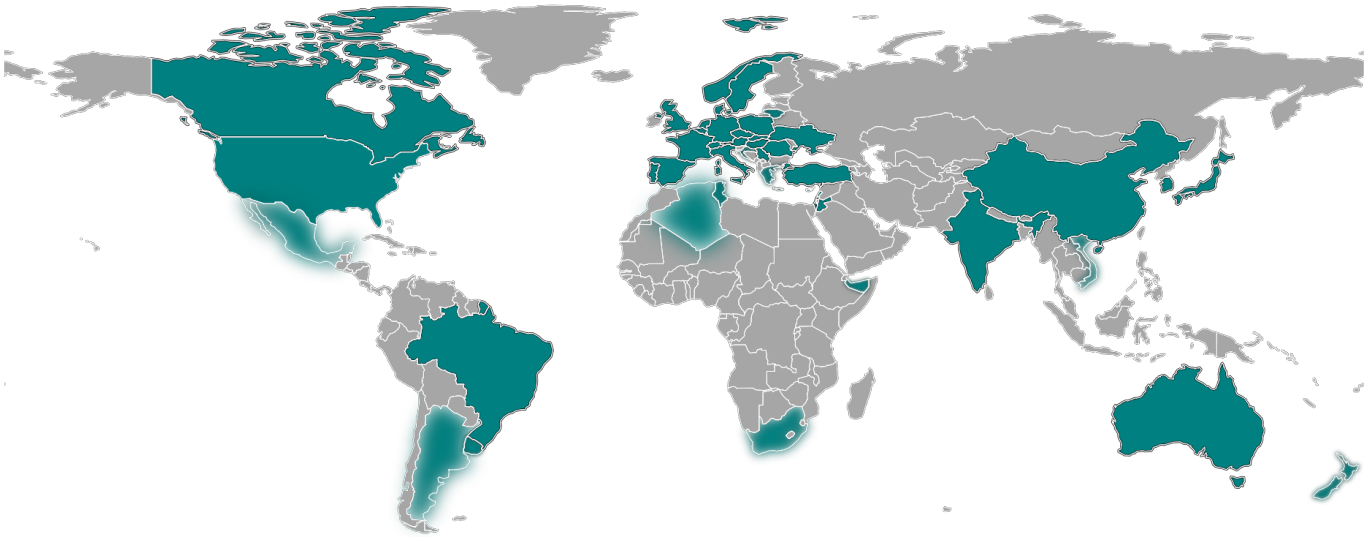

University of New South Wales	Australia
Graz University of Technology	Austria
University of Natural Ressources and Life Sciences Vienna	Austria
Technische Universität Wien	Austria
Belgian Nuclear Research Centre	Belgium
University of Liège	Belgium
Ghent University	Belgium
Universidade de São Paulo	Brazil
University of Ottawa	Canada
Université de Sherbrooke	Canada
Tongji University	China
Qingdao University of Technology	China
Brno University of Technology	Czechia
Czech Technical University	Czechia
University of Pardubice	Czechia
Technical University of Denmark	Denmark
Université Paris-Saclay	France
Karlsruhe Institute of Technology	Germany
University of Stuttgart	Germany
Technical University of Darmstadt	Germany
Leibniz University Hannover	Germany
Dresden University of Technology	Germany
Technical University Munich	Germany
Technische Hochschule Mittelhessen	Germany
Technische Hochschule Würzburg-Schweinfurt	Germany
Technische Universität Berlin	Germany
University of the Bundeswehr Munich	Germany
Budapest University of Technology and Economics	Hungary
Széchenyi István University	Hungary
University of Miskolc	Hungary
Indian Institute of Technology Tirupati	India
Israel Institute of Technology	Israel
Politecnico di Milano	Italy
Politecnico di Torino	Italy
University of Basilicata	Italy
University of Bergamo	Italy
University of Brescia	Italy
University of Rome "Tor Vergata"	Italy
University of Salerno	Italy
Università degli Studi Roma Tre	Italy
The University of Tokyo	Japan
Waseda University	Japan
Yokohama National University	Japan
Budapest University of Technology and Economics	Jordan
Delft University of Technology	Netherlands
University of Stavanger	Norway
Cracow University of Technology	Poland
Silesian University of Technology	Poland
University of Lisbon	Portugal
University of Minho	Portugal
Faculty of Civil Engineering	Serbia
University of Belgrade	Serbia
University of Novi Sad	Serbia
Slovak University of Technology in Bratislava	Slovakia
Seoul National University	South Korea
Polytechnic University of Valencia	Spain
Universitat Politècnica de Catalunya	Spain
Universitat de les Illes Balears	Spain
Linnaeus University	Sweden
ETH Zurich	Switzerland
Istanbul Technical University	Turkey
Istanbul University-Cerrahpasa	Turkey
Yildiz Technical University	Turkey
National University «Yuri Kondratyuk Poltava Polytechnic»	Ukraine
Imperial College London	United Kingdom
University of Leeds	United Kingdom
University of Southampton	United Kingdom
University of Surrey	United Kingdom
Lyles School of Civil Engineering	United States
University of Pretoria	Rep. of South Africa
University of Sfax	Tunisia

Proceedings of the 15th *fib* International PhD Symposium in Civil Engineering

Budapest, Hungary, 28 - 30 August 2024

Edited by

György L. Balázs, Sándor Sólyom, Stephen Foster

fib
CEB-FIP

AZ NKFI ALAPBÓL MEGVALÓSULÓ PROJEKT
NEMZETI KUTATÁSI, FEJLESZTÉSI ÉS INNOVÁCIÓS HIVATAL
AZ INNOVÁCIÓ LENDÜLETE

BME, *consortium leader*
SW Umwelttechnik Mo. Kft.,
ÉMI Nonprofit Kft. MC Bauchemie.
CRH Mo. Kft.

MŰEGYETEM 1782
BUDAPESTI MŰSZAKI ÉS GAZDASÁGTUDOMÁNYI EGYETEM
Építőmérnöki Kar - építőmérnöki képzés 1782 óta
Építőanyagok és Magasépítés Tanszék

National Competitiveness and Excellence Program, Subprogram B:National Program for Materials Science and Technology
Hungarian Research Grant NVKP_16-1-2016-0019
"Development of concrete products with improved resistance to chemical corrosion, fire or freeze-thaw"."
Procurement of laboratory equipment within the framework of the tender entitled

Project supervisor: Prof. György L. Balázs

Project sub-theme responsibles: Dr. Éva Lublóy, Dr. Salem G. Nehme, Dr. Katalin Kopecskó

MATERIAL SCIENTIFIC STUDIES FROM NANO-LEVEL TO MACRO-LEVEL

1. PHENOM XL Scanning Electron Microscope (SEM) with elemental analysis of EDS (energy dispersive X-ray spectroscopy) for small and large (max. 100 mm x 100 mm) samples

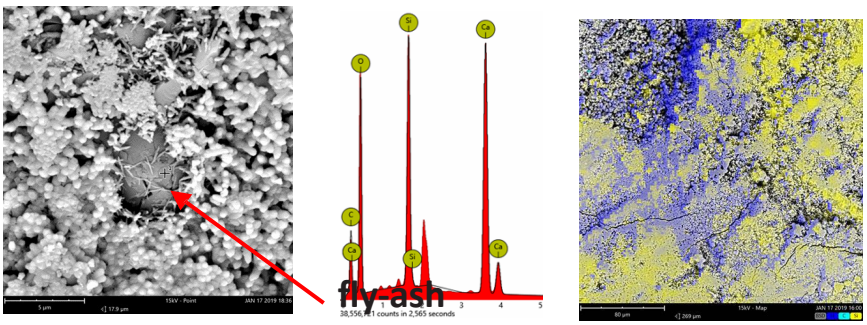

2. TAM Air 3+3 channel microcalorimeter, with 125 ml ampoulles, application range: from cement paste to concrete

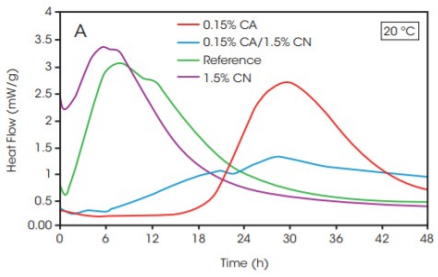

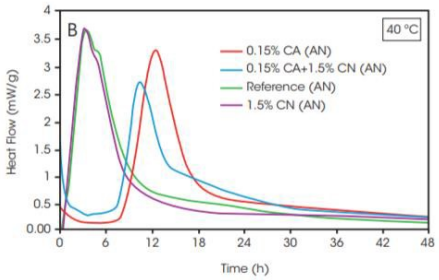

3. Zetasizer Nano ZS – Measurement of Zeta potential with titrator (variable pH range) 3,8 nm – 100 µm, particle size distribution in range 0,3 nm – 10 µm